THE ASTRONOMICAL JOURNAL, 162:176 (20pp), 2021 November https://doi.org/10.3847/1538-3881/ac082a


# The Solar Neighborhood XLVIII: Nine Giant Planets Orbiting Nearby K Dwarfs, and the CHIRON Spectrograph's Radial Velocity Performance

Leonardo A. Paredes[1], Todd J. Henry[2], Samuel N. Quinn[3], Douglas R. Gies[1], Rodrigo Hinojosa-Goñi[4], Hodari-Sadiki James[1], Wei-Chun Jao[1], and Russel J. White[1]
[1] Department of Physics and Astronomy, Georgia State University, Atlanta, GA 30302-4106, USA; lparedes@astro.gsu.edu, gies@chara.gsu.edu, james@astro.gsu.edu, jao@astro.gsu.edu, white@astro.gsu.edu
[2] RECONS Institute, Chambersburg, PA 17201, USA; toddhenry28@gmail.com
[3] Center for Astrophysics, Harvard and Smithsonian, 60 Garden Street, Cambridge, MA 02138, USA; squinn@cfa.harvard.edu
[4] Cerro Tololo Inter-American Observatory, CTIO/AURA Inc., La Serena, Chile; rodrigo.hinojosa@noirlab.edu
*Received 2021 January 6; revised 2021 May 31; accepted 2021 June 2; published 2021 October 4*

## Abstract

We report initial results of a large radial velocity survey of K dwarfs up to a distance of 50 pc from the solar system, to look for stellar, brown dwarf, and Jovian planets using radial velocities from the CHIRON spectrograph on the CTIO/SMARTS 1.5 m telescope. We identify three new exoplanet candidates orbiting host stars in the K dwarf survey and confirm a hot Jupiter from TESS orbiting TOI 129. Our techniques are confirmed via five additional known exoplanet orbiting K dwarfs, bringing the number of orbital solutions presented here to 9, each hosting an exoplanet candidate with a minimum mass of 0.5–3.0 $M_{\mathrm{Jup}}$. In addition, we provide a list of 186 nearby K dwarfs with no detected close companions that are ideal for more sensitive searches for lower-mass planets. This set of stars is used to determine CHIRON's efficiency, stability, and performance for radial velocity work. For K dwarfs with $V = 7$–12, we reach radial velocity precisions of 5–20 $\mathrm{ms}^{-1}$ under a wide range of observing conditions. We demonstrate the stability of CHIRON over hours, weeks, and years using radial velocity standards, and describe instrumental capabilities and operation modes available for potential users.

*Unified Astronomy Thesaurus concepts:* Astronomical techniques (1684); Extrasolar gaseous giant planets (509); Radial velocity (1332); Solar neighborhood (1509); Surveys (1671)

## 1. Introduction

The field of exoplanet discovery has advanced quickly, from the first detections of planets (Latham et al. 1989; Wolszczan & Frail 1992; Mayor & Queloz 1995) to large-scale transit surveys from space transits such as Kepler (Borucki et al. 2010), CoRoT (Baglin et al. 2006), and TESS (Ricker et al. 2014). This paper is concerned primarily with large scale radial velocity (RV) surveys targeting 1000 stars or more, such as the Lick/Keck survey (Butler et al. 2017) and the CORAVEL/HARPS survey (Mayor et al. 2011), which provide key statistics about the formation of stellar and planetary systems. Such large surveys enable ensemble studies to complement individual discoveries, but they are also valuable in the evaluation of observing facilities, techniques, and results. In this spirit, here we provide results from the CHIRON spectrograph on the CTIO/SMARTS 1.5 m (Tokovinin et al. 2013), which is being used as part of a multifaceted survey of more than 5000 of the nearest K dwarfs.

High-resolution spectrographs used for precise RV work are critical components of exoplanet surveys and are particularly relevant now owing to their symbiosis with transit survey instruments on both the ground and in space that are used to detect and characterize planetary systems. In the southern hemisphere there have been at least eight spectrographs precise enough to detect giant planets, operated in various mixtures of classical and queue observations, with or without assistance from the instruments' Principal Investigators (PIs). These instruments include HARPS (Mayor et al. 2003) at ESO La Silla 3.6 m Telescope, FEROS (Kaufer & Pasquini 1998) and CORALIE (former ELODIE; Baranne et al. 1996) at ESO La Silla Swiss 1.2 m Leonhard Euler Telescope, PFS (Crane et al. 2006) and MIKE (Bernstein et al. 2003) at Las Campanas Observatory 6.5 m Magellan II Telescope, FIDEOS (Tala et al. 2014) at ESO La Silla 1 m Telescope, and Veloce Rosso (Gilbert et al. 2018) at the Anglo-Australian Telescope. In this paper, we describe initial science results from our RV search for companions orbiting the nearest K dwarfs carried out at the Cerro Tololo Inter-American Observatory (CTIO) in Chile and provide details about CHIRON operations that are useful for those searching for exoplanets, driven in particular by NASA's TESS mission.

Since 1994, the RECONS group has been studying the nearest stars (Henry et al. 1997), with various scientific investigations focused on horizons spanning 10–100 pc. One of the key results is that the population of stars in the solar neighborhood is dominated by stars smaller than the Sun, with M dwarfs accounting for 75% of all stars, followed by K dwarfs at 12% (Henry et al. 2006, 2018, with updates at www.recons.org). The K dwarfs are the focus of this paper, as they lie in a sweet spot in between the shorter-lived, rarer G dwarfs (5% of the population) and the magnetically active M dwarfs, making them arguably the most suitable hosts for long-term, biologically active planets (Cuntz & Guinan 2016).

In this paper we discuss first results of a survey of several hundred K dwarfs using the CHIRON instrument on the CTIO/SMARTS 1.5 m telescope. CHIRON is being used as part of NASA's efforts to follow-up TESS exoplanet detections and for individual PI spectroscopic surveys of nearby K and M dwarfs. We provide key statistics on the capabilities of CHIRON for K dwarfs with magnitudes of ~8–11 using a set of presumably single stars, resulting in typical RV precisions of 5–20 $\mathrm{ms}^{-1}$. In addition, we present results for giant planets detected orbiting K dwarfs, including (a) five previously known planets used to check our observing

**Table 1**
Modes Available for Observing with CHIRON

| Slit Mode | Binning | $R$ | Throughput | Element Size |
|---|---|---|---|---|
| Fiber | $4 \times 4$ | 28,000 | 1.00 | 4000 $ms^{-1}$ |
| Slicer | $3 \times 1$ | 80,000 | 0.75 | 1000 $ms^{-1}$ |
| Slit | $3 \times 1$ | 90,000 | 0.40 | 1000 $ms^{-1}$ |
| Narrow slit | $3 \times 1$ | 136,000 | 0.20 | 1000 $ms^{-1}$ |

**Note.** The K dwarf survey described in this paper uses slicer mode.

protocols, reduction techniques, and overall CHIRON performance; (b) a detection of a planet orbiting NLTT 58744 (hereafter HIP 65) from TESS (TOI 129); and (c) three candidate planets orbiting the K dwarfs HIP 5763, HIP 34222, and HIP 86221 in our larger survey.

## 2. CHIRON Operations

The CTIO/SMARTS 1.5 m telescope has been operated by the SMARTS Consortium (Subasavage et al. 2010) since 2003. The telescope is primarily operated by on-site CTIO/SMARTS staff observers, although occasional runs are done by individual SMARTS Consortium members. The 1.5 m has had a few different instruments available since SMARTS began, but the primary instrument over the past decade, and the only one operating since 2015, is the CHIRON high-resolution spectrograph (Tokovinin et al. 2013). CHIRON has been operational since 2011, it was upgraded in 2012, and it was used until the 1.5 m closed in 2016, when the primary observing program at the time ended. The 1.5 m was reopened in 2017 June via an effort by RECONS team members Paredes and Henry working closely with CTIO staff members, and the 1.5 m has now been operating exclusively with CHIRON for 3 yr.

### 2.1. Observing Queue Management

Since 2017 June, the RECONS team has overseen the management and operations of the 1.5 m and CHIRON. This includes scientific support, the construction of observing queues, data processing, and data distribution. Queue management is carried out via a web-based platform chiron.astro.gsu.edu, in which time allocations, target requests, desired observing cadences, and on-site telescope operations are fully integrated. Programs from users who purchase observing time and those awarded time via the NOAO/NOIRLab and Chilean TACs are scheduled simultaneously.

Once observing time is allocated, PIs and their collaborators access the queue management platform to submit their targets and observing requirements, managing the use of the observing time that they have been granted. Our queue management team then sorts the various observing requests from multiple PIs to create the nightly schedule, and the observing sequence is executed by a CTIO/SMARTS observer using the same web-based platform. The observer is able to add, remove, or re-sequence observations as sky conditions permit and can complete the arc of some science programs through a seven-night shift or prepare the next shift's observer to carry on longer programs. From 2017 October through 2019 July, the facility was operated every other week; beginning in 2019 August, operations expanded to full-time nightly coverage.

### 2.2. Telescope Operations

A typical night of CHIRON operations starts with a fixed set of calibrations for all observing modes, detailed in Table 1, that commence in the afternoon. At astronomical twilight, the on-site observer accesses the night's observing schedule using the web platform and executes the plan, reporting back the status and/or any issues that may affect the observations. For some programs, an Atlanta-based team member at Georgia State University is available in real time to assist in interpretation of the science requirements. The web platform is directly connected with the instrument controller; therefore, on each target acquired the requested instrument setup is passed directly and efficiently to the instrument and telescope control system (TCS), minimizing time spent and configuration errors. At the end of the night, another fixed set of calibrations is secured. More details are explained in Brewer et al. (2014).

### 2.3. Data Reduction and Distribution

The raw data and calibration files are backed up and transferred for processing daily to computer facilities in Atlanta. The files consist of 2D CCD frames containing the echelle orders and header information, where telescope, ephemerides, spectrograph, and exposure meter (EM) data are recorded. The default data processing consists of bias and flat-field corrections, cosmic-ray removal, echelle order extractions, and wavelength calibrations using ThAr comparison lamps.[5] The algorithms used are based on the REDUCE IDL package (Piskunov & Valenti 2002) and were adapted to CHIRON data with the application of deriving precise RV measurements. Reduced data are produced in FITS file format, containing for each extracted order the flux in photoelectrons and topocentric wavelength in angstroms per pixel. Additional specifics of the data reduction process are described in detail in Tokovinin et al. (2013). Once a night of observations is fully processed, calibration files, raw data, logs, and reduced data are grouped into individual PI programs and placed in secure directories on servers in Atlanta. PIs are then notified and instructed on how to retrieve their data products. Under normal operating conditions, the entire process from raw data acquisition to the delivery of fully processed data products is completed within a few days.

## 3. CHIRON Capabilities

Over the years, the CHIRON spectrograph on the 1.5 m has been used to pursue a wide variety of scientific goals, but it was envisioned as an instrument to measure RVs precise enough to detect planets orbiting bright stars (Giguere et al. 2015). Other science goals accomplished with CHIRON data have involved optical spectral characterization of a variety of astrophysical objects, such as the atmospheres of bright stars and novae (Giguere et al. 2016; Munari & Walter 2016). The results we present here aim to describe the performance capabilities of CHIRON for measuring RVs.

### 3.1. Specifications and Setup Options

CHIRON is able to cover an optical wavelength range between 415 and 880 nm divided into spectral orders from 136

[5] An iodine cell is available, but few CHIRON PIs have used the iodine cell since reopening and wavelength calibrations based on iodine lines are not part of routine operations.

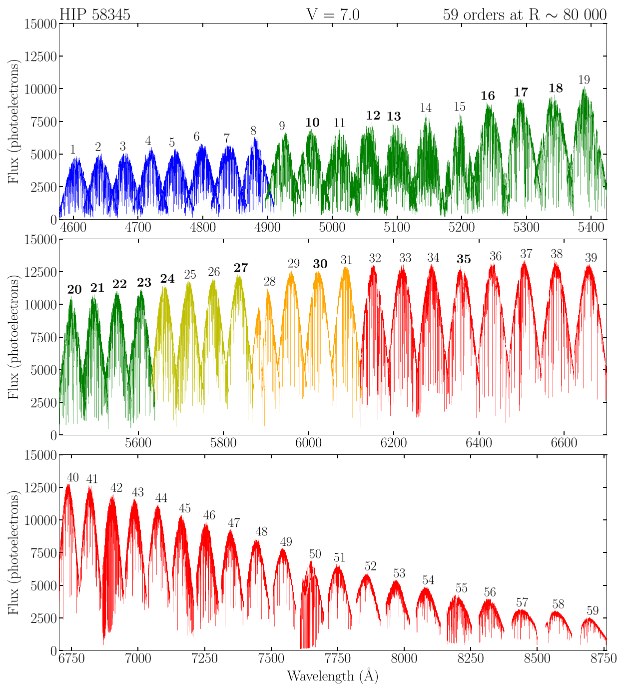

**Figure 1.** 59 echelle spectral orders in slicer mode ($R \sim 80{,}000$) for the K dwarf HIP 58345 extracted by the CHIRON basic reduction pipeline. A fixed set of 14 of these orders (highlighted) are used to derive our RVs.

to 66 and is able to acquire targets up to ∼18 mag through a fiber that is 2.″7 in diameter in the sky. The primary resource for details about CHIRON is Tokovinin et al. (2013), which outlines the four different slit setups available, ranging in resolution from 28,000 to 136,000 (details given in Table 1). A user's choice of setup is dependent on science goals and target brightnesses.

CHIRON offers two wavelength calibration options: a ThAr comparison lamp and an iodine cell. The latter can be used to achieve instrumental precision below 5 $\mathrm{m\,s^{-1}}$ on targets brighter than $V \sim 6$, at the expense of requiring large amounts of observing time to reach a sufficient signal-to-noise ratio (S/N) for such precision. The work we present here utilizes the ThAr lamp for wavelength calibration, which is more versatile than the iodine cell and is the most popular among users.

### 3.2. CHIRON Setup for the K Dwarf Program

The K dwarfs are being observed with CHIRON in slicer mode, which provides a resolution of 80,000 and spreads the spectrum into 59 orders. Integration times are uniformly set to 900 s, except for a few stars brighter than $V \sim 6$, for which the exposure is typically stopped when the S/N reaches 100 at 5500 Å. After each science exposure, a single ThAr lamp exposure of 0.4 s is taken to use for wavelength calibration. In poor seeing or partial cloud cover, the 900 s integration time is maintained in an effort to permit coverage of targets in the large program and to provide insight into how precision changes under various sky conditions. The consistent 900 s integration times for stars with $V \sim 6$–12 also enable straightforward evaluations of the changes in RV precision with magnitude, as well as permitting direct comparisons of fluxes received for individual stars throughout their coverage during the survey.

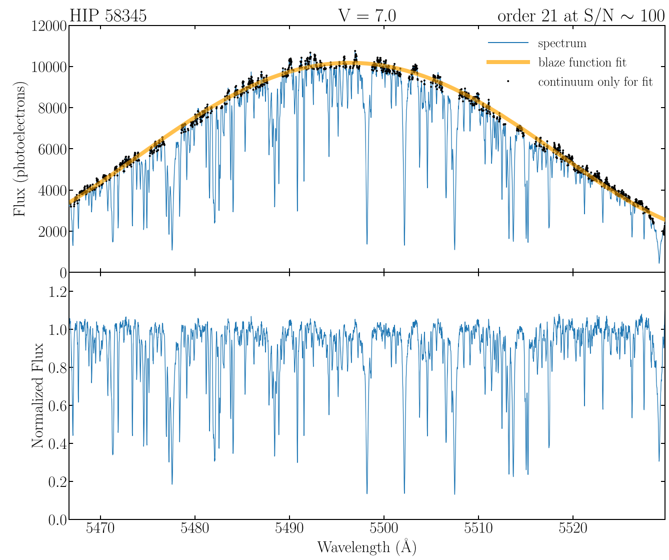

**Figure 2.** Spectrum of order 21 (∼5460–5530 Å) of HIP 58345 taken in slicer mode ($R \sim 80{,}000$) at S/N ∼100. Top: spectrum before the removal of the blaze function, where the black circles are the data points from the original spectrum (blue line) used to fit the blaze function (yellow line). Bottom: normalized spectrum after the removal of the blaze function.

### 3.3. Radial Velocity Pipeline

A pipeline (hereafter the RV pipeline) was developed in Python by this group to process uniformly large volumes of spectra taken with CHIRON to extract RVs. It was optimized specifically for our K dwarf survey at the 1.5 m and follows a recipe that has nine steps.

1. *Input spectra.* Each wavelength-calibrated spectrum (Figure 1) enters the RV pipeline once it has been confirmed to have the proper target identification, as well as correct observational parameters, such as coordinates, hour angle, time of exposure, and air mass.
2. *Flattening spectra.* The removal of the blaze function embedded on each order of echelle spectra is crucial for extracting precise RVs. The Doppler information contained in the spectrum is most valuable in regions where changes in the slope of the flux per wavelength are steepest, i.e., for sharp lines. The flattening process starts with a recursive sigma clipping algorithm to remove the spectral lines over subsections of the order to be able to map the continuum. Subsequently, a fifth-order polynomial is fitted using the remaining data points of the order. Finally, the original unfiltered spectral order is divided by the fitted blaze function to get the flattened normalized version (Figure 2). Removing the blaze function to flatten each order ensures that Doppler shifts are the result of shifting lines due to a star's velocity, rather than from changes in the instrument response along the order. Figure 3 illustrates three spectral regions after removing the blaze function and normalization. These spectral regions include many key features found in K dwarf spectra: Cr I, Fe I, Hα, Li I, Na I, and Ti I.
3. *Barycentric correction.* The motion of Earth around the barycenter of the solar system produces a large (±30 $\mathrm{km\,s^{-1}}$) Doppler oscillation present in all sequences of spectra. These variations must be removed with high precision to derive the final RVs for a targeted star. We use the algorithm "barycorr" by Wright & Eastman (2014),

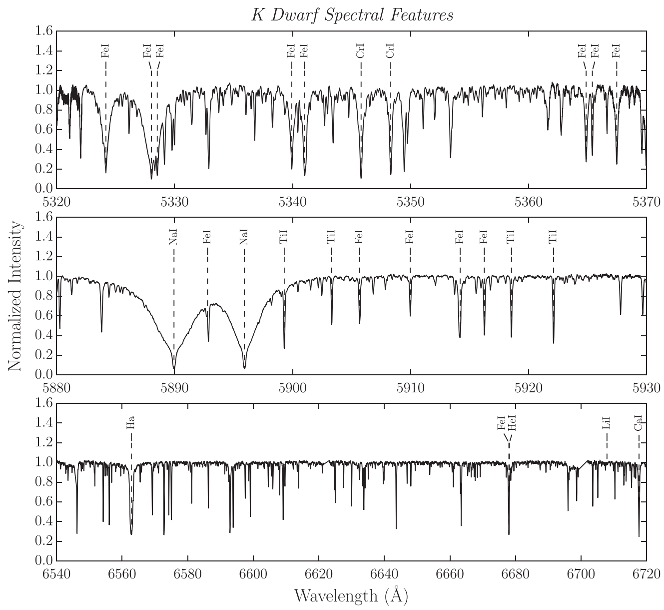


**Figure 3.** Examples of three spectral regions of the K dwarf HIP 73184 observed with CHIRON, after removing the blaze function and normalizing each order.

which calculates corrections appropriate for RV precisions to better than 3 $\mathrm{ms}^{-1}$. The three ingredients used to calculate the correction are (1) the geographical position of the CHIRON spectrograph on Earth, using GPS measurements by Mamajek (2012); (2) the time stamp of the observation, taken as the midpoint of the exposure weighted by photon counts as measured via the exposure meter of CHIRON, saved in the image header under keyword EMMNWOB; and (3) astrometric information for the target star, including its R.A., decl., proper motion, and parallax. For each spectrum a barycentric velocity correction in $\mathrm{ms}^{-1}$ is obtained to be subtracted from the RV derived, and a barycentric Julian date in days is obtained that becomes the time stamp for the corrected RV.

4. *Choose template spectrum.* We calculate an RV at each epoch relative to a single-epoch observation we call the template spectrum for each star. We select the best-quality spectrum as a template, considering weather conditions, Moon illumination, and S/N.
5. *Resample spectrum.* The spectrum is resampled to match the same wavelength grid as the template spectrum to enable direct positional comparisons for the cross-correlation matches. Once the template spectrum is selected, each order is interpolated into a linear log-wavelength grid and oversampled two times the total number of pixels (6400 pixels per order). The result is that any single-pixel Doppler shift across the spectrum corresponds to an RV shift of 500 $\mathrm{ms}^{-1}$ in the slicer mode used for this survey.
6. *Order selection.* One of the advantages of working with spectra from a single spectral type and luminosity class is that spectral features do not vary significantly from one star to another. Therefore, we select a set of spectral orders out of the full set of 59 orders provided by CHIRON on slicer mode that provides the best Doppler results. The quality of the Doppler information given within a single order depends on the number of spectral lines present, the shapes of those lines, the prevalence of telluric lines that pollute the spectrum, and the S/N across the order. Better precision in the RV calculation comes from orders with more numerous spectral lines that are sharp and deep, with few telluric lines, and with less noise. Following these criteria, we omit orders at the extreme ends of the total wavelength range that have relatively low S/N—these are also farthest in wavelength scale from the instrument's peak efficiency at 5500 Å, as well as being relatively far from the blackbody peaks of K dwarfs. In addition, some orders were omitted because they simply have too few lines or are severely contaminated by telluric lines. Finally, orders were removed that have sources of contamination to the RV signal resulting from broad spectral lines and lines sensitive to stellar activity, such as H$\alpha$, H$\beta$, and the Na doublet. In the end, we use a set of 14 orders selected from the 59 available in slicer mode: 10, 12, 13, 16, 17, 18, 20, 21, 22, 23, 24, 27, 30, 35. Note that these are arbitrary order number labels assigned for the reduced data products of CHIRON, where the central wavelength of order $n$ in Å is given by $\lambda_n = 565{,}754/(124 - n)$.
7. *Cross-correlation function.* The RV at a given epoch is calculated relative to the epoch of the selected template spectrum. The wavelength grid of each spectrum is matched to the template spectrum, and then the cross-correlation function (CCF) is calculated for each order pair. The RV derived from the order corresponds to the location of peak of the CCF, for which the location is determined by fitting a Cauchy–Lorentz function. Additional parameters of the fitted function such as FWHM and amplitude are also obtained and used for the uncertainty on the estimated RV.
8. *Uncertainty estimation.* The uncertainty of the RV extracted from each order is closely related to the criteria described in step 6, in concert with the resulting shape of the derived CCF. We estimate a velocity uncertainty for a single order following the prescription by Zucker (2003) by quantifying the relative amplitude and sharpness of its CCF. The CCF shape and quality are directly related to the S/N of the spectrum; therefore, the errors estimated this way are photon errors. Instrumental errors and astrophysical noise are not reflected in this value, so the quoted errors may underestimate the total uncertainty.
9. *RV calculation.* Once each order from a given spectrum is cross-correlated with its respective order in the template, a final RV and its uncertainty are computed as in step 7. The final value and uncertainty for the epoch's observation are derived using the individual values and their uncertainties from the 14 orders by determining a weighted mean value and the standard error on the weighted mean.

### 3.4. CHIRON Stability

Here we provide details about the stability of CHIRON on three timescales: over a night, a month, and the more than 2 yr since the 1.5 m was reopened. Three K dwarf standard stars, HIP 3535 ($V = 8.0$), HIP 58345 ($V = 7.0$), and HIP 73184 ($V = 5.8$), have been observed since the telescope was reopened in 2017 June, and combined, two (HIP 3535 and HIP 58345) now provide a consistent stream of data, as they compensate for one another's seasonal gaps. These three stars

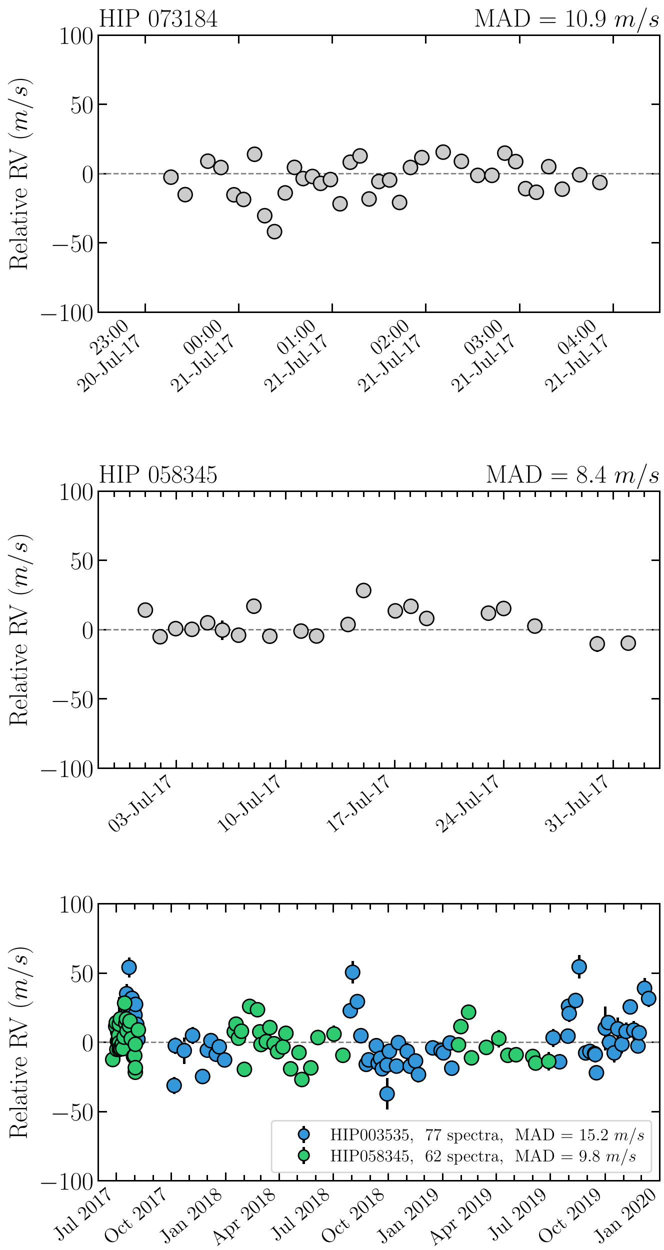


**Figure 4.** Three K dwarfs used as RV standards to monitor the stability of CHIRON. Top: HIP 73184 observed for ~4.5 hr on a single night. Middle: HIP 58345 observed roughly once per night for a month; skipped nights were due to unfavorable weather conditions. Bottom: HIP 3535 and HIP 58345 observed between 2017 June and 2019 December with a typical cadence of one observation every 7–10 days.

were selected because they had data from previous RV programs indicating that they have variations of only 3–7 $\mathrm{ms}^{-1}$ over years (Butler et al. 2017), sufficiently low for our purposes to consider them RV standard stars. Results for all three stars are shown in Figure 4 and with RV data listed in Table A1. There are occasional outlier points, in particular for HIP 3535, the faintest of the three standards.

The error associated with each RV measured on a night is tightly correlated with the photon flux received by the CHIRON detector and relates to the variance across the 14 orders for which individual RVs are extracted, but as can be seen in the time series for HIP 3535, for example, the dispersion as measured by the mean absolute deviation (MAD) of the points overall (15 $\mathrm{ms}^{-1}$) is larger than errors on most of the individual points (typically 3–10 $\mathrm{ms}^{-1}$). The roughly factor of two difference is presumably due to systematic errors, with the leading culprits being changes in the focus of lines on the CCD and temperature fluctuations inside the chamber that houses the CHIRON instrument.

Once multiple spectra are available for a given star, the MAD is calculated for all available spectra, which is ~0.8 times the standard deviation of normally distributed data. It is the MAD values for various stars that are given in the panels of Figure 4 and reported henceforth in this paper. We emphasize that these results are for K dwarfs observed during our survey; other types of stars will not necessarily provide similar results, i.e., hotter stars with fewer lines available for RV extraction, or rapidly rotating stars with broad lines.

1. *Stability over hours:* HIP 73184 was observed 36 times on the night of 2017 July 17 to test the stability of CHIRON over a period of ~4.5 hr. Observations were taken on a clear night with seeing of $0\farcs7$–$1\farcs0$, while the air mass changed from 1.012 to 1.674. The top panel of Figure 4 shows that the MAD is 10.9 $\mathrm{ms}^{-1}$ during the series of observations.
2. *Stability over 1 month:* As shown in the middle panel of Figure 4, HIP 58345 was observed on 21 nights over a 1 month period in 2017. There are few RV measurements lying far from the mean value, with a resulting MAD of 9.8 $\mathrm{ms}^{-1}$ for the data series. This MAD is likely lower than that for HIP 3535 on a single night simply because HIP 58345 is a magnitude brighter in *V*.
3. *Stability over 2+ yr:* The bottom panel of Figure 4 includes data sequences for HIP 3535 (77 spectra, MAD value 15.2 $\mathrm{ms}^{-1}$) and HIP 58345 (62 spectra, MAD 9.8 $\mathrm{ms}^{-1}$) together, as observations are dovetailed throughout the year to provide an unbroken series of RV standard observations. It is evident that there are several stretches of time when RV offsets are found in the HIP 3535 data sequence. We have examined various quantities in an attempt to reveal the cause(s) of the offsets for individual measurements. It appears that the drifts in the HIP 3535 data are *not* caused solely by (a) varying S/N in the spectra (primarily because nearly all spectra, 62 out of 77, have S/N > 50; out of the 15 RVs where the S/N is below 50, only four deviate by more than 15 $\mathrm{ms}^{-1}$ from the mean), (b) air mass, and (c) temperature changes in the coudé room where CHIRON is housed. We suspect that the poorer precision is due to shifts in the final spectral resolution: values computed from the individual spectra indicate that when the resolution dips by more than ~1%, the final RV points are offset. Resolution offsets occur when the focus of the spectrum onto the CCD drifts slightly, and this shows that it is critical to keep the lines consistently as narrow as possible on the chip. In addition, we find a correlation between the most deviated RVs from the mean (>15 $\mathrm{ms}^{-1}$) and their individual uncertainties. This is consistent with the fact that our error bars reflect mostly photon noise in combination with instrumental errors, but having bright stars in this case, the latter reason seems to dominate.

In summary, for K dwarfs with $V = 7$–12, the data indicate that CHIRON is stable to 5–20 $\mathrm{ms}^{-1}$ over timescales of hours, 1 month, and more than 2 yr.

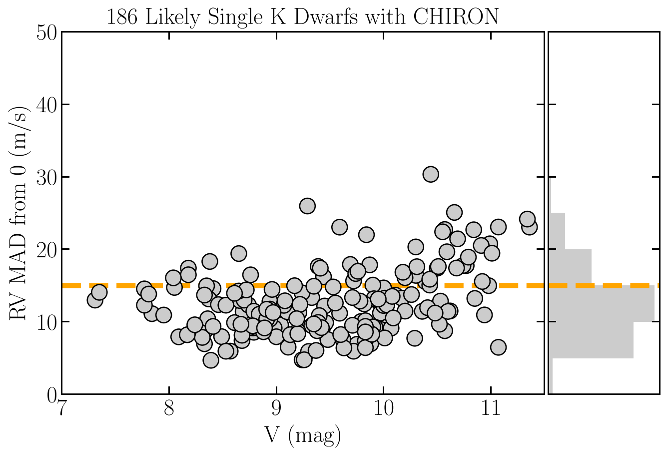


**Figure 5.** Dependence of the scatter in the RV time series on the $V$ magnitude for each of the 186 K dwarfs with no Keplerian RV signal (Table A3). The right panel groups data points in bins of 5 ms$^{-1}$, indicating that 75% of RV MADs are below 15 ms$^{-1}$ (dashed line), with the best series as low as 5 ms$^{-1}$.

## 4. K Dwarf Survey and Observations

### 4.1. Sample

The observed stars are a portion of an effort targeting more than 5000 K dwarfs within 50 pc; details about the full sample will be given in a future paper in this series. The particular subset observed here includes 190 stars selected from Hipparcos (van Leeuwen 2007) to have parallaxes of at least 30 mas, placing them within 33 pc of the Sun, and that have decl. between +30° and −30°. This equatorial sample has been selected so that each star can be observed from major observatories in both hemispheres. Sample star observations began before Gaia Data Release 2 (Evans et al. 2018) results were available; hence, stars closer than the sample horizon entered the observing list using Hipparcos parallaxes.

Stars of spectral type K were chosen using an assessment of the regions where dividing lines between the G/K and K/M spectral types are found, with types determined by Gray & Corbally (2009) and RECONS. To define the blue and red ends of the K dwarf sequence, stars with spectral types were matched to members of the RECONS 25 pc sample that have been carefully vetted for close companions, enabling us to use presumably single stars uncorrupted by close companions to map K dwarf spectral types to $V-K$ colors. We find that K dwarfs span $V-K=1.90$–3.70, and we apply an additional constraint of $M_V=5.80$–8.80 to eliminate evolved stars and white dwarfs. The $V-K$ values were accumulated for the sample stars using $V$ from Tycho (Høg et al. 2000) and $K$ from the Two Micron All Sky Survey (2MASS; Skrutskie et al. 2006). The resulting list of 300 stars includes 110 that have stellar companions (either published by others or to be published by us) and/or have at least 10 RV measurements found in the data archives of HARPS (Mayor et al. 2003) and HIRES (Vogt et al. 1994). The remaining 190 stars compose the sample discussed here and are (a) within 33 pc, (b) located in the equatorial region of the sky, (c) have colors and absolute magnitudes of K dwarfs, and (d) have not been observed extensively, if at all, in previous RV programs.

The sample is presented in Table A3, including 186 K dwarfs for which no companion has been detected with RV and four stars with new Jovian exoplanet candidates. In addition, we provide results for nine more stars: one K dwarf from TESS discovered to have a planet, five K dwarfs with previously known planet candidates used as checks on our observing and reduction methodologies, and the three K dwarfs used as RV standards discussed in Section 3.4. For all 199 stars, Table A3 provides names, coordinates, $V$ photometry from Tycho (Høg et al. 2000), $K_s$ photometry from 2MASS (Skrutskie et al. 2006), $B_g$ and $R_g$ photometry from Gaia (Evans et al. 2018), the number and time coverage of the RV observations, and the MAD values for the RV series.

### 4.2. Observations and Radial Velocity Precision

Our RV search is designed to perform a systematic reconnaissance for companions, so each K dwarf in our sample gets at least six, and ideally nine, observations using the slicer instrument setup described in Section 3.2. The observing cadence goal is to secure two to three spectra within 7 days, then repeat the sequence after a month, and then repeat it again after a year. The MAD values for the sequences of spectra for 186 stars for which we do not find periodic RV variations with CHIRON are illustrated in Figure 5 and listed in Table A3. Given that Jupiter-mass planets in (edge-on) orbits with periods of 10–100 days around K dwarfs cause RV variations of ∼40–100 ms$^{-1}$, it is clear that CHIRON is precise enough to detect Jupiter-mass exoplanets orbiting virtually all of the targeted K dwarfs.

For observational planning, it is useful to examine CHIRON's precision as a function of target brightness. Figure 5 illustrates the dependence of the scatter for the RV time series using the MAD values versus $V$ magnitudes of the K dwarfs whose RV curve is flat, i.e., they do not show periodic variation or a trend in their RVs over time. For our observing and data reduction protocols, we reach precisions of 5–15 ms$^{-1}$ for $V=7.0$–10.5, with slightly poorer precision for $V=10.5$–11.5; therefore, the points above ∼20 ms$^{-1}$ in the plot may, in fact, be as-yet-unidentified perturbations or young active stars, and they may be worthy of a closer look; additional observations are planned for these stars.

In addition to mapping the dependence of RV precision with target brightness, because sky conditions and telescope tracking vary, it is useful to map the precision as a function of the S/N for individual spectra (as measured by CHIRON's exposure meter during an observation). Figure 6 relates the S/N values for 1784 individual spectra of the 186 K dwarfs to the resulting RV uncertainties. Overall, for S/N values of at least 40, the uncertainties are less than 15 ms$^{-1}$, whereas for S/N ∼20, the uncertainties increase to 30 ms$^{-1}$ and above. It is therefore recommended that to reach a precision of 15 ms$^{-1}$ in slicer mode with CHIRON, observers targeting K dwarfs or similar stars anticipate exposure times of 900 s (our standard exposure time) for stars with $V \lesssim 10.5$. As a rule of thumb, to obtain a single measurement error in RV of ∼5 ms$^{-1}$, it is necessary to reach S/N ∼ 100 at 5500 Å. This is possible for a K dwarf brighter than $V\sim9$ in 900 s exposure in slicer mode. Overall, for stars like those observed in our program, the expected precision can be predicted using

$$\sigma_{\rm RV} \sim \frac{10,000}{{\rm S/N}^2} + 4\ {\rm ms}^{-1}. \tag{1}$$

The S/N of each spectrum is computed using the counts from the exposure meter, which picks off about 1% of the collimated light at 5450 Å with a bandwidth of 900 Å (Tokovinin et al. 2013). This S/N value maps directly to the

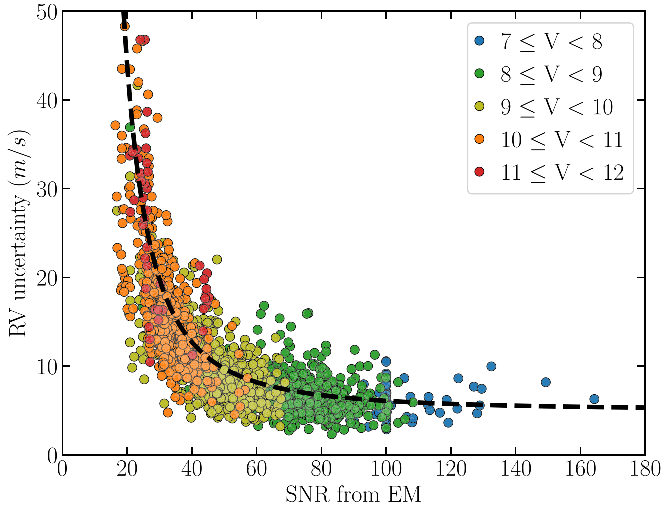


**Figure 6.** S/N calculated from CHIRON's exposure meter (EM) vs. RV uncertainty for individual spectra, color-coded by stellar $V$ magnitude. Each of the 1784 data points represents a single spectrum. The dashed line is described by Equation (1) and is derived using observations with exposure times of 900 s. The slight overabundance of points at $S/N = 100$ is the result of observations that were stopped before 900 s, when the S/N reached 100.

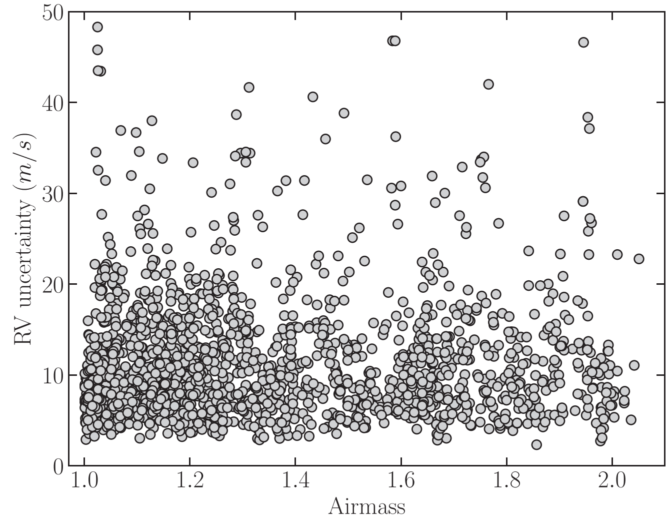


**Figure 7.** Air mass versus RV uncertainty per spectrum. Typically, targets are observed when they are close to the meridian passage, but this is not always possible owing to scheduling constraints. It is clear that RV uncertainty is not systematically affected by the air mass at which the K dwarfs have been observed.

S/N of the raw spectra and provides a straightforward method to evaluate individual exposures. Importantly, the S/N can be tracked by an observer during an exposure to compensate for cloud cover, seeing, and telescope tracking, all of which can affect how much light is injected into the fiber. As a result, an observer can actively stop or extend an integration to reach a desired S/N. For example, the collection of vertical points at $S/N = 100$ represents observations of relatively bright stars for which exposures were stopped before 900 s. The relation to convert from exposure meter counts to S/N is given by

$$S/N = \sqrt{\frac{EMNUMSMP \times EMAVG - 7401.973}{57.909}}, \tag{2}$$

where *EMNUMSMP* is the number of samples of a tenth of a second during the exposure and *EMAVG* is the average instant number of photon counts during the exposure; both are recorded as header entries with these names for each spectrum taken.

As outlined in Section 3.3, the individual RV measurements have been determined using the weighted standard error of the RVs measured for the 14 orders adopted in the pipeline. While there are other errors, such as systematic instrumental offsets to be considered in future work when larger data sets are available, for this characterization of our K dwarf survey prospects we report errors that are only the result of the statistical results based on individual RVs extracted from the 14 different orders. As expected, the RV errors are lower for brighter stars and higher-S/N spectra.

Finally, because our sample stars span decl. $= -30°$ to $+30°$, we observe stars with air masses of 1.0–2.0 from CTIO. Although not every observation is timed precisely when a star passes through the meridian, most observations occur near transit, and a plot of air mass versus RV uncertainty is useful to understand whether or not high air-mass observations yield lower RV precision. Figure 7 illustrates that the RV uncertainty is independent of the air mass, a result that is particularly encouraging because stars north of decl. = 0 can be observed with CHIRON as effectively as more southern stars. This also bodes well for individual targets for which many observations are desired over the span of a single night, given that RV uncertainties are consistent over a large range of air mass.

## 5. Results

Over the past two decades, more than 4300 planets orbiting other stars have been detected and confirmed (as listed in the NASA Exoplanet Archive, exoplanetarchive.ipac.caltech.edu as of 2021 May), including more than 3300 revealed via the exoplanet transit method. The greatest contributor of transiting exoplanets has been the Kepler mission (Borucki et al. 2010), which was extended via the K2 effort (Howell et al. 2014). Together, Kepler and K2 have revealed thousands of exoplanet candidates, and TESS continues to add to the candidate list. Among the finds are terrestrial, ice giant, and gas giant planets, with orbital periods ranging from hours to years. Most relevant to the work presented here, given the precision of CHIRON and the duration of the survey, are planet candidates with masses of $0.3\ M_{\rm Jup} < m \sin i < 10\ M_{\rm Jup}$ and orbital periods of $P < 180$ days. As of 23) 2021 May, a search of the NASA Exoplanet Archive yields 93 stellar hosts within 100 pc with at least one confirmed exoplanet that meets these criteria.

Many of the exoplanets revealed during the transit surveys are followed up using RVs to confirm that the object is, indeed, a planet orbiting the star identified to exhibit the transit. In addition, there have been more than 800 candidates detected during RV surveys that do not transit. Here we discuss nine K dwarfs that are orbited by low-mass companions that are exoplanet candidates. A total of 240 individual measured RVs from CHIRON are given for these nine stars in Table A2, ordered by Hipparcos number.

The orbital fits for all nine systems are shown in Figure 8. Our orbits have been derived using the code Systemic2 (Meschiari et al. 2009),[6] which provides a functional interface that can be used to calculate Lomb–Scargle periodograms and to explore orbital fits interactively given a set of RV data. All plots have zero phase defined to be at the epoch of periastron. Our calculated RVs are input into the code, and the

[6] github.com/stefano-meschiari/Systemic2

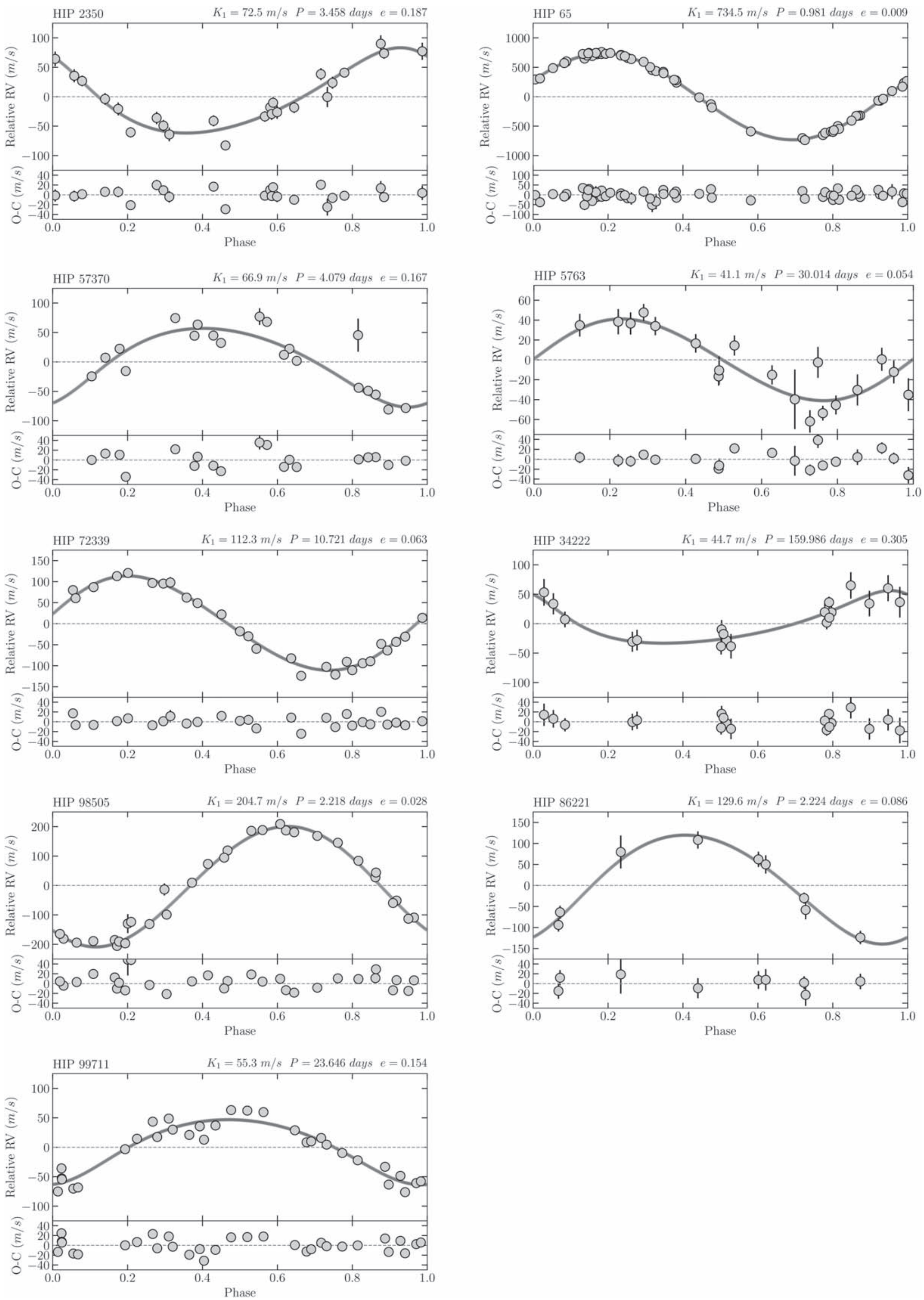


**Figure 8.** Phase-folded RV curves and residuals derived from CHIRON spectra. Phase zero indicates the time of the periastron passage ($T_p$). Left column: five planets known to orbit K dwarfs. Right column: four new planet candidates around K dwarfs.

periodogram is inspected for prominent peaks above the 10% false-alarm probability (FAP) level. We avoid those peaks that match the nightly cadence and total baseline of the observations because they are caused by sampling aliases. Keplerian orbits are then fit for each of ∼5 strongest peaks and the results inspected by eye. Initial fits are made using circular orbits in

**Table 2**
Orbital Parameters of Exoplanet Candidates

| Star | $M_*$ $M_\odot$ | Period (days) | $m \sin i$ ($M_{\rm Jup}$) | $e$ | $\omega$ (deg) | $K$ (ms$^{-1}$) | $a$ (au) | $T_p$ (JD −2,450,000) | rms (ms$^{-1}$) | Data Points | References |
|---|---|---|---|---|---|---|---|---|---|---|---|
| Previously Known Exoplanet Systems | | | | | | | | | | | |
| HIP 2350 | 0.92 | $3.458^{+0.0081}_{-0.0083}$ | 0.50 | 0.187 | 37.28 | $72.5^{+4.6}_{-4.4}$ | 0.044 | 7948.482 | 12.8 | 24 | this work |
| | 0.93 | 3.444 | 0.48 | 0.000 | 126.90 | 67.4 | 0.044 | 3323.206 | ⋯ | 28 | Moutou et al. (2005) |
| HIP 57370 | 0.92 | $4.079^{+0.0142}_{-0.0146}$ | 0.49 | 0.167 | 206.16 | $66.9^{+3.5}_{-3.3}$ | 0.049 | 7933.659 | 26.1 | 20 | this work |
| | 0.93 | 4.114 | 0.49 | <0.140 | 143.40 | 63.4 | 0.049 | 3732.700 | 16.0 | 59 | Ge et al. (2006) |
| HIP 72339 | 0.85 | $10.721^{+0.0033}_{-0.0031}$ | 1.09 | 0.063 | 281.05 | $112.3^{+4.6}_{-4.5}$ | 0.090 | 7928.965 | 9.9 | 28 | this work |
| | 0.79 | 10.720 | 1.02 | 0.044 | 203.63 | 115.0 | 0.088 | 1287.380 | 15.4 | 118 | Udry et al. (2000) |
| HIP 98505 | 0.84 | $2.218^{+0.0010}_{-0.0009}$ | 1.17 | 0.028 | 136.42 | $204.7^{+2.6}_{-2.5}$ | 0.031 | 7929.288 | 21.5 | 31 | this work |
| | 0.82 | 2.219 | 1.15 | 0 (fix) | ⋯ | 205.0 | 0.031 | ⋯ | ⋯ | 35 | Bouchy et al. (2005) |
| HIP 99711 | 0.74 | $23.646^{+0.2304}_{-0.2082}$ | 0.63 | 0.154 | 188.21 | $55.3^{+2.1}_{-2.2}$ | 0.146 | 7912.820 | 13.5 | 32 | this work |
| | 0.75 | 24.348 | 0.72 | 0 (fix) | 0.00 | 61.0 | 0.150 | ⋯ | ⋯ | 182 | Santos et al. (2003) |
| TESS Exoplanet System | | | | | | | | | | | |
| HIP 65 | 0.74 | 0.981 (fix) | 2.95 | 0.009 | 291.42 | $734.6^{+4.6}_{-4.5}$ | 0.017 | 8368.833 | 20.4 | 58 | this work |
| | 0.78 | 0.981 | 3.21 | 0 (fix) | ⋯ | 753.7 | 0.017 | ⋯ | ⋯ | 34 | Nielsen et al. (2020) |
| New Candidate Exoplanet Systems | | | | | | | | | | | |
| HIP 5763 | 0.72 | $30.014^{+0.1528}_{-0.2842}$ | 0.51 | 0.054 | 271.08 | $41.1^{+8.8}_{-11.2}$ | 0.170 | 8056.731 | 16.2 | 19 | this work |
| HIP 34222 | 0.62 | $159.986^{+2.6753}_{-2.9256}$ | 0.83 | 0.305 | 31.80 | $44.7^{+9.1}_{-8.3}$ | 0.492 | 8023.220 | 12.7 | 19 | this work |
| HIP 86221 | 0.79 | $2.224^{+0.0004}_{-0.0005}$ | 0.71 | 0.086 | 208.93 | $129.6^{+34.5}_{-19.6}$ | 0.031 | 7947.283 | 12.8 | 9 | this work |

order to avoid very high eccentricity orbits that may fit the data sets but are astrophysically unlikely. Step sizes of 0.001 days are used to fine-tune the orbital period, while the fitting process is carried out using chi-square minimization until each orbit fit converges, determined when the rms of the fit reaches ∼20 ms$^{-1}$. We have chosen this limit given the typical RV scatter and uncertainties seen for the 186 K dwarfs with no detected companions, as shown in Figures 5 and 6. As a final step in the orbital parameter determinations, we derive the intervals of confidence for parameters using MCMC simulations also included in the Systemic2 code, starting with the model best fitted, a total of ∼10,000 steps, in two chains, and skipping the first 1000 iterations. Errors are not listed for previous orbital parameters because they are a mix of different types of errors.

Table 2 includes the orbital parameters and errors for all nine K dwarf + exoplanet systems highlighted here. To estimate the companion $m \sin i$ values, masses for the primary stars have been derived using $V$ magnitudes converted from $V_T$ magnitudes (Høg et al. 2000) and the mass–luminosity relation in $M_V$ of Henry & McCarthy (1993). A future paper is planned to provide a much-needed update to the mass–luminosity relation for K dwarfs using empirically determined masses.

### 5.1. Known Planets Orbiting K Dwarfs

Here we provide five examples of previously known planet candidates orbiting K dwarfs revealed via RVs. All five are (presumed) single-planet systems chosen during the initial reopening of the CTIO/SMARTS 1.5 m in 2017 June to serve as test targets to verify the efficacy of CHIRON under typical observing protocols. The instrument setup, data reduction, and RV calculation methods were as described in Sections 3.1–3.3 for all of the stars. Each of the new orbital solutions presented here has been calculated solely based on the CHIRON observations and therefore is independent of previously reported solutions found in the literature.

#### 5.1.1. HIP 2350

This star ($V = 9.37$, K1V) was reported by Moutou et al. (2005) to have a hot Jupiter of minimum mass 0.48 $M_{\rm Jup}$ with an orbital period of 3.444 days. We obtained 24 spectra of HIP 2350 between 2017 July 16 and August 08 and confirm a 0.50 $M_{\rm Jup}$ minimum-mass planet with an orbital period of 3.458 days, consistent with the previous result. The 73 ms$^{-1}$ RV semiamplitude is ∼7 times larger than the typical uncertainty for K dwarfs in our program, indicating that hot Jupiters of this type are easily revealed by CHIRON. HIP 2350 has a lower-mass stellar companion detected with RoboAO at Palomar (Baranec et al. 2012) at a separation of 0.″5 and fainter by 3.3 mag at 754 nm (Sloan i' filter) by Riddle et al. (2015) and Roberts et al. (2015). The companion was confirmed with DSSI at Gemini North (Horch et al. 2009) at a separation of 0.″5 and fainter by 3.8 mag at 692 nm (Wittrock et al. 2016). The companion is likely an M1V with an estimated orbital period of ∼130 yr from the projected separation, and it should not pose a serious threat to the detection, nor the orbital stability of the planet. Shaya & Olling (2011) and later Oh et al. (2017) reported HIP 2350 to be part of a comoving wide pair where the primary component is HIP 2292, another solar-type star, at projected separation of 897″ (∼0.2 pc). While the system could still be a wide multiple, Oh et al. (2017) also discuss the possibility that systems such as these could have formed together but are now drifting apart.

#### 5.1.2. HIP 57370

This star ($V = 8.05$, K0V) was reported by Ge et al. (2006) to have a hot Jupiter with a minimum mass 0.49 $M_{\rm Jup}$ in an orbit with a period of 4.114 days. We obtained 20 spectra of HIP 57370 between 2017 June 29 and 2017 July 26, and with the same minimum mass of 0.49 $M_{\rm Jup}$ in an orbital period of 4.079 days. The single point with a large error near phase 0.8 in the panel for this star in Figure 8 was taken at the beginning of the night on 2017 July 26, when clouds were present and the seeing expanded to 2″5, resulting in poor S/N for this observation. This data point is included to illustrate the relative quality of a poor observation suffering from high photon noise error compared to more typical measurements. The lack of speckle companions (Nusdeo et al. 2018) or any known visual stellar companions makes this detection robust. Despite being a nontransiting planet, Guilluy et al. (2019) use this hot Jupiter (HD 102195 b) to demonstrate the feasibility of detailed studies of exoplanet atmospheres using the GIANO spectrograph (Oliva et al. 2006) mounted at Telescopio Nazionale Galileo (TNG), a 4 m class telescope.

#### 5.1.3. HIP 72339

This star ($V = 8.04$, K0V) is near the celestial equator, but at $V - K_s = 1.81$ it is slightly bluer than the blue cutoff we used for our K dwarf sample; thus, it is not part of the larger survey but was observed strictly as a benchmark. This star has a known hot Jupiter with minimum mass 1.02 $M_{\rm Jup}$ and orbital period 10.720 days (Udry et al. 2000). We confirm the companion via 28 spectra to have a somewhat larger minimum mass of 1.02 $M_{\rm Jup}$ and a virtually identical orbital period of 10.721 days. Our phased RV curve spans 3.5 full orbits for data taken in 2017 from June 24 to August 7, and this is the star with a known planet for which we have the longest time coverage at 42 days. Given the RV variation caused by the companion of $K = 112$ ms$^{-1}$, this Jupiter-like planet is clearly detected, indicating that CHIRON reveals such candidates easily. No visual stellar companions are known in the system, and the planet is not found to be transiting. While this system has been revisited by Wittenmyer et al. (2009) and Hinkel et al. (2015), the candidate exoplanet's properties have not changed significantly since the initial discovery.

#### 5.1.4. HIP 98505

We obtained 31 observations of HIP 98505 ($V = 7.66$, K2V) between 2017 June 24 and August 4, spanning 40 days, to reveal a companion with minimum mass 1.17 $M_{\rm Jup}$ in a 2.218-day orbit. This planet (HD 189733 b) was discovered by Bouchy et al. (2005) and reported to have a minimum mass of 1.15 $M_{\rm Jup}$ in a 2.219-day orbit; the system has been extensively studied since then with no significant changes in the orbital parameters. At an orbital inclination of ~85°, the exoplanet transits its host star, allowing detailed determination of its fundamental parameters, which, combined with the proximity and brightness of the star, have made the system an ideal laboratory for exoplanet atmosphere studies (e.g., Redfield et al. 2008; Guilluy et al. 2020, and references therein). Bakos et al. (2006) report a lower-mass companion 11″2 from HIP 98505 that is 3.7 mag fainter in $K_s$. Using astrometry, proper motion, RV, and photometry, they derive an orbit for the stellar companion nearly perpendicular to the planet's transiting orbit, i.e., nearly face-on. However, at a projected separation of 218 au and orbital period of 3200 yr, the orbit is highly uncertain.

#### 5.1.5. HIP 99711

We found for this star ($V = 7.76$, K2V) a 0.63 $M_{\rm Jup}$ companion with the longest orbital period (23.646 days) and the smallest RV amplitude (55.3 ms$^{-1}$) of the five selected benchmark stars. Nonetheless, the RV perturbation is clear in the CHIRON data, and the values are close-enough matches to those in the discovery paper (Santos et al. 2000). The companion (HD 192263 b) is among the earliest exoplanet candidates but was called into question by Henry et al. (2002), who argued that the RV signal detected is due to stellar magnetic activity rather than the stellar reflex motion caused by a companion. However, Santos et al. (2003) then provided further proof to improve the planet's orbit and confirmed the discovery, which is also supported by our measurements. We suspect that the difference in the orbital solution we found is due to contamination of the RV signal by the same stellar magnetic activity that initially disputed the discovery.

### 5.2. New Planets Orbiting K Dwarfs

Here we discuss four candidates for giant planets orbiting nearby K dwarfs, including a contemporaneous detection of a transiting exoplanet from TESS and three new candidate exoplanets from our survey.

#### 5.2.1. TESS Target HIP 65 (NLTT 57844)

A possible low-mass companion was found to transit HIP 65 (TOI 129, $V = 11.13$, K4V) in the first set of data released from TESS in sector 2, and later in sectors 28 and 29. At 61.9 pc, this star is beyond the 50 pc cutoff of our K dwarf survey but was observed as an early possible discovery by TESS that could be quickly verified with CHIRON data. Initial RVs were collected with CHIRON starting on 2018 September 8, and within 2 weeks of the first TESS data release.[7] The quick turnaround was possible because of the nimble system established to acquire CHIRON observations. A total of 58 spectroscopic observations have been secured between 2018 September 8 and 2020 January 12, and we find an RV signal consistent with the TESS transit signal detected. Our analysis yields a giant planet companion with mass 2.95 $M_{\rm Jup}$ in an orbital period of 0.981 days, consistent with the orbit published by Nielsen et al. (2020). The properties of the ~1 day orbit and massive planet make this an excellent candidate for detailed exoplanet atmospheric studies.

#### 5.2.2. HIP 5763

This K dwarf survey star ($V = 9.86$, K6V) shows a perturbation with a period of 30 days in the RVs due to a companion with minimum mass 0.51 $M_{\rm Jup}$. A total of 19 observations spanning 2 yr were secured between 2017 November 20 and 2019 December 17. This planet candidate has the smallest RV amplitude (41.1 ms$^{-1}$) of the four new detections reported here, but this amplitude is clearly offset from results for stars of similar brightness in Figure 5, indicating that the companion is likely real. In addition, the rms of the residuals to the orbital fit (16.2 ms$^{-1}$) is similar to the rms values we find after fitting orbits for the five known planetary systems. HIP 5763 is not known to have visual stellar companions reported in the Washington Double Star Catalog (WDS; Mason et al. 2001), nor any spectroscopic binary companions reported in The Ninth Catalogue of Spectroscopic Binary Orbits (SB9; Pourbaix et al. 2004). TESS observed this target in sector 17 from 2019 October 8 to 2019 November 2 (25 days) at 2-minute cadence; the TESS SPOC (Science Processing Operations Center) pipeline does not report transit events.

[7] An orbit was published at www.recons.org on 2018 September 10.

### 5.2.3. HIP 34222

At $V = 10.23$, this K7V star is one of the fainter K dwarfs in the sample, which is reflected in the relatively large error bars on individual points. We obtained 19 spectra spread over 2 yr between 2017 December 15 and 2019 December 18. The data set indicates a possible companion with minimum mass 0.83 $M_{\rm Jup}$ in an orbit with $e = 0.301$, which is the most eccentric of the nine systems discussed here. With a derived orbital period of 160 days, the relatively high eccentricity is not precluded by tidal circularization, which happens only for systems with orbital periods less than a few weeks (Halbwachs et al. 2005); nonetheless, we consider this to be the least precise orbit presented here. The WDS reports WDS J07057+2728B as a visual companion 4.6 mag fainter at 13.5″, but no parallax or reliable proper motion is available to confirm that it is bound to HIP 34222. Although WDS lists five stars as nearby, none are physical companions. No spectroscopic companion is listed in the SB9 catalog.

### 5.2.4. HIP 86221

This star ($V = 9.20$, K5V) is among the most northern in our equatorial sample, with decl. $\sim +28°$. We find a classic hot Jupiter candidate in a 2.2-day orbit with minimum mass 0.71 $M_{\rm Jup}$. Although we have only nine observations to date for this star, the semiamplitude of the orbital fit, 130 m s$^{-1}$, is more than 10 times CHIRON's typical MAD value for K dwarfs of this brightness, so we consider the detection secure. The HIP 86221 system is known to be a stellar triple. The AB components are separated by a few tenths of an arcsecond, with B fainter than A by 0.59 mag in the optical. A visual binary orbit has been determined for AB using astrometry and speckle interferometry, yielding a period of 23.991 yr, semimajor axis of 0$''$.2884, and eccentricity 0.2053 (Mason et al. 1999; Söderhjelm 1999; Malkov et al. 2012). No spectroscopic companion is listed in the SB9 catalog. Thus, the companion we detect is not the stellar secondary and presumably orbits the primary given that the flux in the spectra is heavily weighted to the brighter primary component. The third star in the system is NLTT 45161 at a distance of 9$''$.4 and is 2.26 mag fainter in the $V$ band than the combined AB pair (Mason et al. 2001; Gould & Chanamé 2004). Among FGK dwarf systems, 12% are triple-star systems (Raghavan et al. 2010; Tokovinin 2014), and as of 37) 2021 May the NASA Exoplanet Archive reports 3260 stellar systems hosting at least one confirmed exoplanet, of which 41 are triple-star systems, making this detection rare among the known exoplanet population.

Table 2 summarizes the orbital elements for the nine systems discussed here. The values listed include the first orbits from the discovery references and our orbit. We have not added any points from other efforts to ours from CHIRON to enable direct comparisons between results. For the five stars used to check the veracity of our observing and reduction efforts with CHIRON, we find that our orbits are in good agreement with those found in the discovery papers. We note that we have been able to reach similar orbital solutions with less data compared to the discovery papers, primarily because of CHIRON's RV precision for this type of star.

### 5.3. K Dwarfs for Future Low-mass Planet Surveys

In Table A3, we also provide details for the 186 K dwarfs within 50 pc for which no companion down to our sensitivity and time coverage has been detected. In addition to names and epoch/equinox 2000.0 coordinates, each star's parallax from Gaia DR2, $V$ and $K$ photometry, $V - K$ color, and $M_V$ magnitude are given, as well as the number of observations and time span of our CHIRON observations.

Note that companions farther than a few au from their primaries are beyond the sensitivity limit of our RV survey to date—we hope to reveal most stellar companions at these separations through our high-resolution speckle survey of the same stars. The 186 stars listed should become high-priority targets for terrestrial planet searches because we now know that they do not have stellar or brown dwarf companions within a few au. In fact, cross-checks of the NASA Exoplanet Archive as of 2021 May have revealed that none of the 186 stars have confirmed planets. However, additional checks of K2 and TESS reveal that four—HIP 5286, HIP 11707, HIP 12493, and HIP 74981—have recently been added to the TESS TOI list. Still, none of these stars have significant numbers of observations in the HARPS and HIRES data archives, so each remains a promising new target for deeper and more precise searches for terrestrial planets.

## 6. Conclusions

We have presented the first results of our ongoing RV survey of nearby K dwarfs with the CHIRON spectrograph. Three K dwarf RV standard stars and a set of 186 stars with no detected companions have been used to determine the stability level of CHIRON over 2.5 yr to be 5–20 m s$^{-1}$ for K dwarf stars with magnitudes of $V = 7$–12. Previously known planets around five K dwarfs have been independently detected with CHIRON and produced orbital solutions consistent with previous efforts. We have independently confirmed a giant planet around a K dwarf initially discovered by TESS, taking data with CHIRON within a few days of the first TESS data release. Three K dwarfs in our survey show RV variations consistent with planets of minimum masses from 0.5–0.9 $M_{\rm Jup}$ in orbital periods of 2–160 days. We provide details for 186 K dwarfs within 50 pc that do not show significant variations in RV indicative of close stellar or substellar companions in orbits with periods less than a year. Vetting stars for close brown dwarf and Jovian companions is a time-consuming and expensive effort in the search for terrestrial exoplanets; thus, we provide this list of K dwarfs as ideal targets for extreme precision RV programs.

All of the K dwarfs in our survey are also being examined for stellar companions; as promising new multiple stellar systems show up in our data with larger RV variations, long-term RV linear trends, and fully resolved orbits, we are preparing them for the next publication. Moreover, beyond the few au regime sampled by the RV effort, both high-resolution speckle imaging and wide-field companion searches are being done to provide a comprehensive assessment of stellar companions from 0 to 1000 au, which will ultimately provide a detailed understanding of where stellar companions form around K dwarfs and what their orbital architectures look like. Because of its sensitivity, the RV survey probes beyond stellar companions to brown dwarf and massive planetary companions, providing an opportunity to evaluate architectures for all three classes of companions.

Via a carefully defined sample with systematic coverage in three spatial regimes, we will be able to reveal the results of the stellar, brown dwarf, and Jovian planetary formation processes, with an ultimate expansion to the regime of terrestrial planets.

In the end, we will then understand the populations of companions spanning a factor of ∼1000 in mass for many of the nearest K dwarfs to the Sun.

This work has been supported by the National Science Foundation via grants AST-1517413 and AST-1910130. We are indebted to members of the SMARTS Consortium and NSF's National Optical-Infrared Astronomy Research Laboratory, particularly the staff at CTIO, for efforts to keep the 1.5 m and the CHIRON spectrograph in operation. At CTIO, Rodrigo Hinojosa, Roberto Aviles, Hernan Tirado, Manuel Hernandez, David Rojas, Javier Rojas, Humberto Orrego, Esteban Parkes, Marco Bonati, Peter Moore, Nicole David, Mauricio Rojas, Andrei Tokovinin, Steve Heathcote, Ximena Herreros, Luz Pinto, Rodrigo Hernandez, Jacqueline Seron, Fernando Cortes, Carlos Corco, Alberto Miranda, Jorge Briones, Jorge Lopez, Pedro Ramos, Alfonso Rojas, Hector Pasten, Juan Paleo, Marco Nunez, and so many others. We also want to thank Eric Mamajek for his insightful comments on this work. This research has made use of the NASA Exoplanet Archive, which is operated by the California Institute of Technology, under contract with the National Aeronautics and Space Administration under the Exoplanet Exploration Program. This publication makes use of data products from the Two Micron All Sky Survey, which is a joint project of the University of Massachusetts and the Infrared Processing and Analysis Center/California Institute of Technology, funded by the National Aeronautics and Space Administration and the National Science Foundation. This work has made use of data from the European Space Agency's Hipparcos mission and Gaia (cosmos.esa.int/gaia) mission, the latter processed by the Gaia Data Processing and Analysis Consortium (DPAC, cosmos.esa.int/web/gaia/dpac/consortium). Funding for the DPAC has been provided by national institutions, in particular the institutions participating in the Gaia Multilateral Agreement.

*Facilities:* CTIO:1.5 m, TESS, Exoplanet Archive.

## Appendix

Additional tables.

**Table A1**
CHIRON Radial Velocities of K-Dwarf Radial-velocity Standards

| BJD − 2,450,000 (days) | RV ($\mathrm{m\,s^{-1}}$) | $\sigma_{\mathrm{RV}}$ ($\mathrm{m\,s^{-1}}$) |
|---|---|---|
| | HIP 003535 | |
| 7937.93779 | 3.6 | 4.5 |
| 7952.91229 | 31.3 | 6.9 |
| 7953.91139 | 12.0 | 3.6 |
| 7955.89438 | 19.4 | 4.3 |
| 7956.89693 | 50.4 | 7.1 |
| 7957.88705 | 4.0 | 3.4 |
| 7958.89154 | 21.0 | 4.9 |
| 7959.89157 | 3.1 | 3.4 |
| 7960.90567 | 16.3 | 3.5 |
| 7961.89886 | 28.0 | 5.5 |
| 7964.86529 | 15.7 | 4.7 |
| 7964.87851 | −5.1 | 4.8 |
| 7964.89314 | 19.3 | 8.3 |
| 7966.88038 | 15.9 | 4.7 |
| 7967.87161 | 23.6 | 2.5 |
| 7968.84481 | 5.6 | 3.4 |
| 7969.84934 | 9.2 | 4.1 |
| 7971.82710 | −1.6 | 2.9 |
| 8032.72070 | −34.9 | 6.1 |
| 8034.70148 | −6.1 | 5.8 |
| 8049.70544 | −9.7 | 9.4 |
| 8063.66741 | 1.3 | 6.0 |
| 8080.58239 | −28.4 | 3.3 |
| 8088.55321 | −9.4 | 3.9 |
| 8094.56871 | −2.5 | 4.4 |
| 8103.56055 | −12.4 | 4.1 |
| 8108.56269 | −7.0 | 5.7 |
| 8117.53255 | −16.5 | 4.8 |
| 8328.87868 | 19.0 | 3.5 |
| 8332.81382 | 46.8 | 8.0 |
| 8340.85366 | 25.6 | 2.2 |

**Table A1**
(Continued)

| BJD − 2,450,000 (days) | RV ($ms^{-1}$) | $\sigma_{RV}$ ($ms^{-1}$) |
|---|---|---|
| 8346.74116* | 1.0 | 4.9 |
| 8355.76342 | −19.6 | 1.8 |
| 8359.77765 | −16.4 | 3.9 |
| 8372.74307 | −6.2 | 5.0 |
| 8375.74388 | −18.8 | 3.8 |
| 8379.71874 | −15.3 | 4.3 |
| 8382.68316 | −22.9 | 4.4 |
| 8390.75122 | −40.9 | 11.2 |
| 8390.75869 | −20.1 | 5.6 |
| 8394.64051 | −10.2 | 5.8 |
| 8406.71501 | −20.9 | 4.7 |
| 8409.75878 | −4.0 | 4.7 |
| 8424.58772 | −10.3 | 6.9 |
| 8429.60039 | −21.0 | 4.2 |
| 8438.58231 | −17.2 | 4.6 |
| 8443.57756 | −27.0 | 5.4 |
| 8467.56317 | −7.8 | 4.5 |
| 8481.54435 | −9.7 | 5.6 |
| 8485.53214 | −11.4 | 2.8 |
| 8496.54465 | −4.2 | 4.3 |
| 8499.54251 | −22.4 | 5.2 |
| 8669.94105 | −0.5 | 6.4 |
| 8680.87636 | −17.8 | 5.0 |
| 8694.86469 | 0.7 | 4.4 |
| 8695.91882 | 22.3 | 3.8 |
| 8696.94116 | 17.0 | 6.1 |
| 8707.83373 | 26.4 | 3.0 |
| 8713.74162 | 50.7 | 8.4 |
| 8724.73160 | −11.4 | 4.7 |
| 8731.76619 | −10.3 | 5.3 |
| 8739.66745 | −11.9 | 5.1 |
| 8740.78399 | −12.6 | 5.7 |
| 8742.76074 | −25.7 | 5.1 |
| 8757.72640 | 6.4 | 15.9 |
| 8762.72234 | 10.5 | 5.6 |
| 8764.74822 | −3.8 | 5.2 |
| 8772.63562 | −11.4 | 6.8 |
| 8778.72172 | 6.0 | 8.3 |
| 8785.64313 | −5.1 | 6.6 |
| 8792.64111 | 4.1 | 6.2 |
| 8799.66675 | 21.8 | 4.6 |
| 8805.59900 | 5.1 | 6.6 |
| 8812.59844 | −6.4 | 4.5 |
| 8814.58366 | 3.1 | 5.1 |
| 8823.64221 | 35.2 | 7.5 |
| 8830.56459 | 27.9 | 6.1 |
| HIP 058345 | | |
| 7929.47227 | −23.1 | 3.4 |
| 7934.51183 | 1.0 | 4.1 |
| 7935.50558 | 3.5 | 5.3 |
| 7936.45360 | −15.7 | 3.3 |
| 7937.44903 | −9.9 | 3.4 |
| 7938.49311 | −10.4 | 2.0 |
| 7939.50140 | −5.7 | 3.9 |
| 7940.44767 | −10.9 | 7.0 |
| 7940.46230 | −15.7 | 8.0 |
| 7940.47513 | 2.4 | 19.6 |
| 7941.48157 | −14.6 | 2.7 |
| 7942.46453 | 6.3 | 5.5 |
| 7943.48651 | −15.4 | 4.2 |
| 7945.48714 | −11.6 | 4.1 |
| 7946.48332 | −15.2 | 5.3 |
| 7948.50122 | −6.9 | 2.6 |

**Table A1**
(Continued)

| BJD − 2,450,000 (days) | RV ($ms^{-1}$) | $\sigma_{RV}$ ($ms^{-1}$) |
|---|---|---|
| 7949.50256 | 17.6 | 4.5 |
| 7951.53332 | 3.0 | 3.3 |
| 7952.53421 | 6.2 | 3.9 |
| 7953.54595 | −2.5 | 2.7 |
| 7957.50429 | 1.3 | 3.7 |
| 7958.48138 | 4.7 | 5.2 |
| 7960.48108 | −8.0 | 3.0 |
| 7964.47982 | −20.9 | 5.7 |
| 7966.46944 | −20.3 | 3.9 |
| 7967.46667 | −32.2 | 5.0 |
| 7967.47976 | −12.0 | 3.5 |
| 7967.48817 | −29.0 | 5.9 |
| 7972.46397 | −1.7 | 3.8 |
| 8133.86703 | −3.0 | 4.2 |
| 8136.84237 | 2.5 | 4.7 |
| 8140.87425 | −7.6 | 3.4 |
| 8145.87504 | −2.6 | 4.7 |
| 8150.85799 | −30.2 | 3.3 |
| 8159.74411 | 15.3 | 3.6 |
| 8172.86354 | 12.9 | 3.6 |
| 8176.73761 | −3.1 | 5.2 |
| 8178.79027 | −12.2 | 2.2 |
| 8187.69472 | −10.1 | 2.7 |
| 8193.71248* | 0.0 | 3.9 |
| 8200.71629 | −11.7 | 1.0 |
| 8206.66241 | −17.4 | 4.6 |
| 8215.63786 | −14.0 | 2.4 |
| 8220.62637 | −4.1 | 1.2 |
| 8228.64657 | −29.8 | 2.0 |
| 8242.64360 | −18.0 | 3.4 |
| 8247.53488 | −37.5 | 4.4 |
| 8262.54488 | −29.1 | 5.2 |
| 8274.55207 | −7.2 | 4.8 |
| 8301.49704 | −4.7 | 6.0 |
| 8316.45984 | −20.0 | 4.5 |
| 8510.82843 | −12.4 | 3.7 |
| 8514.89015 | 0.7 | 3.0 |
| 8527.80571 | 11.1 | 1.6 |
| 8532.69755 | −21.8 | 4.4 |
| 8557.64528 | −14.3 | 2.6 |
| 8578.67044 | −7.9 | 6.3 |
| 8593.76299 | −20.0 | 3.4 |
| 8607.69268 | −19.6 | 4.1 |
| 8635.68290 | −20.9 | 3.4 |
| 8640.58051 | −25.6 | 3.9 |
| 8662.59434 | −24.4 | 6.5 |
| HIP 073184 | | |
| 7929.57864 | 4.1 | 1.6 |
| 7934.58382 | 0.1 | 4.1 |
| 7935.59031 | 26.6 | 3.6 |
| 7936.56410 | 10.1 | 2.1 |
| 7937.55489 | 14.3 | 3.2 |
| 7938.57440 | −7.3 | 2.6 |
| 7939.58877 | 16.4 | 3.0 |
| 7941.51141 | 19.2 | 0.4 |
| 7942.55522 | −17.4 | 1.2 |
| 7943.54831 | −26.7 | 2.2 |
| 7945.53189 | 4.8 | 4.3 |
| 7946.54298 | 27.8 | 2.4 |
| 7948.57620 | 6.0 | 3.6 |
| 7949.53540 | 11.7 | 2.1 |
| 7951.61597 | −11.5 | 2.7 |
| 7952.57729 | −1.2 | 2.0 |

**Table A1**
(Continued)

| BJD − 2,450,000 (days) | RV ($m s^{-1}$) | $\sigma_{RV}$ ($m s^{-1}$) |
|---|---|---|
| 7954.50028 | 9.3 | 2.4 |
| 7954.54084 | 10.5 | 2.6 |
| 7954.57675 | −14.6 | 0.9 |
| 7954.61224 | −21.6 | 4.5 |
| 7954.64590 | 11.3 | 1.6 |
| 7954.68161 | −7.5 | 0.5 |
| 7955.61843* | 7.5 | 2.3 |
| 7957.53453 | −4.9 | 1.7 |
| 7958.51432 | −10.0 | 2.7 |
| 7959.52758 | 6.3 | 3.8 |
| 7960.52905 | 4.1 | 2.8 |
| 7964.50926 | −8.3 | 1.2 |
| 7966.50109 | −25.1 | 1.8 |
| 7969.53070 | 14.6 | 4.2 |
| 7971.52182 | 2.9 | 2.3 |
| 7971.52730 | −0.8 | 3.3 |
| 7972.57029 | −24.3 | 1.2 |
| 7972.57641 | −1.5 | 3.3 |
| 7973.49741 | −11.6 | 3.3 |
| 7974.59661 | −14.3 | 2.8 |
| 7984.46368 | 19.0 | 2.2 |
| 7985.47296 | −14.6 | 3.4 |
| 7986.46875 | −7.7 | 2.3 |
| | HIP 073184 within a Night | |
| 7955.46977 | −9.8 | 2.1 |
| 7955.47611 | −22.4 | 0.3 |
| 7955.48620 | 1.7 | 2.6 |
| 7955.49203 | −2.8 | 3.6 |
| 7955.49781 | −22.5 | 1.7 |
| 7955.50210 | −25.9 | 2.7 |
| 7955.50700 | 6.7 | 0.1 |
| 7955.51153 | −37.6 | 3.4 |
| 7955.51589 | −49.1 | 2.9 |
| 7955.52064 | −21.2 | 0.7 |
| 7955.52477 | −2.7 | 0.8 |
| 7955.52862 | −10.8 | 3.0 |
| 7955.53277 | −9.3 | 0.7 |
| 7955.53641 | −14.3 | 2.3 |
| 7955.54078 | −11.5 | 0.7 |
| 7955.54507 | −29.0 | 3.0 |
| 7955.54961 | 1.0 | 1.4 |
| 7955.55396 | 5.5 | 2.2 |
| 7955.55799 | −25.5 | 3.0 |
| 7955.56236 | −12.9 | 1.6 |
| 7955.56714 | −11.8 | 1.0 |
| 7955.57157 | −28.1 | 2.3 |
| 7955.57642 | −2.8 | 1.7 |
| 7955.58148 | 4.3 | 2.2 |
| 7955.59099 | 8.3 | 1.5 |
| 7955.59910 | 1.6 | 1.8 |
| 7955.60639 | −8.5 | 1.0 |
| 7955.61269 | −8.5 | 0.9 |
| 7955.61843* | 7.5 | 2.3 |
| 7955.62327 | 1.4 | 1.6 |
| 7955.62768 | −18.1 | 1.8 |
| 7955.63247 | −20.7 | 3.2 |
| 7955.63798 | −2.2 | 0.8 |
| 7955.64400 | −18.4 | 2.5 |
| 7955.65179 | −8.1 | 2.7 |
| 7955.66077 | −13.7 | 1.3 |

**Note.** (*) marks the reference epoch.

**Table A2**
CHIRON Radial Velocities of Known and New Planet Candidates

| BJD − 2,450,000 (days) | RV ($m s^{-1}$) | $\sigma_{RV}$ ($m s^{-1}$) |
|---|---|---|
| | HIP 002350 | |
| 7951.89442 | 77.2 | 14.5 |
| 7952.90012 | −36.1 | 10.6 |
| 7953.89963 | −33.5 | 9.0 |
| 7955.88144 | −3.8 | 10.0 |
| 7956.88370 | −41.0 | 9.4 |
| 7957.87499 | 38.4 | 10.2 |
| 7958.87913 | 64.3 | 12.4 |
| 7959.87877 | −49.2 | 9.6 |
| 7960.86503 | −17.9 | 9.3 |
| 7960.87869* | −29.3 | 10.1 |
| 7960.89144 | −10.2 | 9.2 |
| 7961.88615 | 90.1 | 14.1 |
| 7964.85088 | −0.5 | 17.2 |
| 7966.84962 | −64.1 | 11.6 |
| 7967.84517 | −26.3 | 11.2 |
| 7968.83282 | 73.7 | 9.2 |
| 7969.83590 | −20.7 | 11.0 |
| 7970.82671 | −82.8 | 8.5 |
| 7971.81477 | 23.7 | 10.2 |
| 7972.88795 | 35.6 | 11.1 |
| 7974.91900 | −18.2 | 9.5 |
| 7983.78358 | −60.5 | 8.7 |
| 7985.75744 | 40.9 | 7.1 |
| 7986.79379 | 26.8 | 9.1 |
| | HIP 057370 | |
| 7934.45458 | −15.5 | 6.1 |
| 7935.49137 | 32.3 | 8.2 |
| 7937.50350 | −78.3 | 5.4 |
| 7938.46593 | 22.5 | 6.4 |
| 7939.48726 | 44.7 | 7.2 |
| 7944.47423 | 1.9 | 6.0 |
| 7945.47259 | −81.0 | 6.4 |
| 7946.46890 | 7.2 | 5.7 |
| 7947.47382 | 63.4 | 5.3 |
| 7948.47416 | 22.4 | 5.0 |
| 7951.51847 | 44.5 | 6.1 |
| 7952.49357 | 12.0 | 6.2 |
| 7953.49230* | −55.5 | 6.1 |
| 7954.47789 | −24.5 | 4.6 |
| 7957.48911 | −49.1 | 7.6 |
| 7959.46760 | 74.5 | 5.8 |
| 7960.46572 | 68.0 | 6.6 |
| 7961.45805 | 45.5 | 28.2 |
| 7961.46449 | −44.0 | 5.4 |
| 7964.46424 | 76.9 | 14.2 |
| | HIP 072339 | |
| 7929.54565 | 79.9 | 7.2 |
| 7934.56758 | −29.9 | 6.7 |
| 7936.54942* | −108.8 | 6.2 |
| 7937.54107 | −110.7 | 5.8 |
| 7938.54737 | −63.7 | 4.8 |
| 7939.54678 | 13.8 | 5.2 |
| 7941.52488 | 113.1 | 4.5 |
| 7942.54093 | 96.7 | 5.1 |
| 7943.51842 | 62.1 | 4.6 |
| 7944.52069 | 22.1 | 6.6 |
| 7945.51703 | −59.8 | 7.3 |
| 7946.51391 | −82.3 | 5.4 |
| 7947.52004 | −102.7 | 6.5 |
| 7948.56045 | −94.2 | 5.0 |

**Table A2**
(Continued)

| BJD − 2,450,000 (days) | RV ($ms^{-1}$) | $\sigma_{RV}$ ($ms^{-1}$) |
|---|---|---|
| 7949.51980 | −43.4 | 5.7 |
| 7951.57622 | 87.0 | 6.1 |
| 7952.56338 | 120.6 | 5.6 |
| 7953.57462 | 95.4 | 5.3 |
| 7954.55280 | 49.0 | 4.1 |
| 7957.52048 | −124.1 | 7.1 |
| 7958.49852 | −121.2 | 7.1 |
| 7959.50038 | −89.5 | 6.9 |
| 7960.49920 | −30.8 | 8.0 |
| 7964.49635 | 98.0 | 12.8 |
| 7966.48701 | −18.1 | 5.5 |
| 7969.54572 | −90.4 | 5.4 |
| 7970.53248 | −48.1 | 7.5 |
| 7972.50529 | 60.7 | 5.7 |
| HIP 098505 | | |
| 7929.73335 | −129.5 | 32.4 |
| 7933.78957 | −180.9 | 5.2 |
| 7934.76108 | 119.0 | 6.5 |
| 7935.76221 | −51.3 | 4.9 |
| 7936.76874 | 9.5 | 5.7 |
| 7937.75467 | 84.0 | 5.4 |
| 7941.76233 | 187.0 | 5.9 |
| 7942.74095 | −194.3 | 6.6 |
| 7943.77564 | 185.7 | 5.0 |
| 7944.73933 | −109.1 | 4.4 |
| 7945.73698 | 73.3 | 6.5 |
| 7946.72916 | 27.8 | 3.9 |
| 7947.69775 | −13.5 | 20.6 |
| 7948.72484 | 145.3 | 6.2 |
| 7949.71869 | −123.7 | 10.7 |
| 7951.71345 | −189.0 | 7.5 |
| 7952.71563 | 188.3 | 4.7 |
| 7953.73393 | −164.7 | 5.0 |
| 7954.70688 | 94.6 | 5.8 |
| 7955.70707 | −59.6 | 4.7 |
| 7958.70140 | −131.2 | 3.3 |
| 7959.69553 | 168.6 | 4.3 |
| 7960.71401 | −185.4 | 3.8 |
| 7960.72722⋆ | −205.4 | 5.3 |
| 7960.73934 | −190.8 | 3.3 |
| 7961.69405 | 208.8 | 5.7 |
| 7964.67201 | −113.0 | 2.9 |
| 7966.69832 | 43.9 | 6.5 |
| 7967.67659 | −99.1 | 4.3 |
| 7969.64983 | −196.7 | 5.9 |
| 7970.65065 | 180.9 | 4.5 |
| HIP 099711 | | |
| 7928.85159 | 8.4 | 5.8 |
| 7929.77375 | 15.8 | 5.3 |
| 7933.80559 | −33.2 | 3.6 |
| 7934.77486 | −48.6 | 3.5 |
| 7935.77614 | −60.9 | 4.1 |
| 7936.79664 | −75.1 | 5.2 |
| 7937.76887 | −70.3 | 3.4 |
| 7941.78987 | 14.5 | 3.3 |
| 7942.78353 | 43.5 | 4.6 |
| 7943.79578 | 48.7 | 4.1 |
| 7945.75133 | 35.5 | 3.5 |
| 7946.74455 | 37.0 | 6.3 |
| 7947.73203 | 63.2 | 4.5 |
| 7948.75327 | 62.3 | 4.0 |

**Table A2**
(Continued)

| BJD − 2,450,000 (days) | RV ($ms^{-1}$) | $\sigma_{RV}$ ($ms^{-1}$) |
|---|---|---|
| 7949.77388 | 59.7 | 4.0 |
| 7951.75601 | 28.8 | 6.8 |
| 7952.78594 | 10.0 | 5.2 |
| 7953.76042 | 4.4 | 4.9 |
| 7954.74812 | −9.8 | 5.5 |
| 7955.72372 | −22.1 | 4.3 |
| 7957.68199 | −63.4 | 4.8 |
| 7958.71591 | −76.3 | 4.0 |
| 7959.71218 | −57.9 | 2.7 |
| 7960.66741 | −35.8 | 2.2 |
| 7960.67976 | −52.9 | 3.4 |
| 7960.69186⋆ | −54.5 | 4.1 |
| 7961.70835 | −68.4 | 3.9 |
| 7964.68627 | −3.3 | 5.7 |
| 7966.71242 | 17.5 | 3.4 |
| 7967.69067 | 30.0 | 4.3 |
| 7968.73616 | 20.9 | 4.4 |
| 7969.66455 | 12.9 | 3.6 |
| HIP 000065 | | |
| 8369.59230 | −650.8 | 16.5 |
| 8369.68969 | −319.3 | 12.2 |
| 8369.74174 | −67.4 | 11.9 |
| 8369.81965 | 293.6 | 13.4 |
| 8370.57894 | −613.7 | 11.7 |
| 8370.66590 | −323.7 | 12.9 |
| 8370.71827⋆ | −65.7 | 16.7 |
| 8370.78546 | 234.8 | 15.2 |
| 8371.57496 | −591.1 | 15.4 |
| 8371.64147 | −326.5 | 16.7 |
| 8371.77372 | 265.9 | 11.8 |
| 8371.82794 | 486.0 | 10.1 |
| 8371.92226 | 744.7 | 15.3 |
| 8372.56158 | −597.2 | 22.3 |
| 8372.69277 | −36.1 | 9.6 |
| 8372.84314 | 590.3 | 7.0 |
| 8372.92524 | 722.9 | 20.5 |
| 8373.55514 | −499.4 | 19.9 |
| 8373.69723 | 96.9 | 38.4 |
| 8375.55321 | −406.1 | 16.5 |
| 8375.78704 | 600.6 | 16.4 |
| 8375.86988 | 742.4 | 14.0 |
| 8379.61043 | 171.5 | 19.8 |
| 8379.78845 | 740.0 | 15.7 |
| 8380.62274 | 309.9 | 16.9 |
| 8380.78421 | 726.7 | 12.0 |
| 8380.91677 | 453.0 | 35.9 |
| 8381.90793 | 435.4 | 39.1 |
| 8382.90787 | 423.1 | 19.0 |
| 8383.88954 | 399.8 | 19.0 |
| 8385.88544 | 240.0 | 16.7 |
| 8390.59432 | 758.4 | 21.6 |
| 8390.78867 | 278.6 | 25.0 |
| 8392.68328 | 504.0 | 13.5 |
| 8393.51258 | 692.4 | 17.6 |
| 8393.58814 | 712.3 | 10.7 |
| 8394.50312 | 743.9 | 31.1 |
| 8394.58626 | 659.7 | 15.1 |
| 8394.80467 | −127.8 | 13.8 |
| 8395.51021 | 729.3 | 22.2 |
| 8404.71885 | −589.5 | 15.9 |
| 8509.54996 | −11.6 | 11.6 |
| 8799.62251 | 648.2 | 26.2 |

**Table A2**
(Continued)

| BJD − 2,450,000 (days) | RV ($m s^{-1}$) | $\sigma_{RV}$ ($m s^{-1}$) |
|---|---|---|
| 8800.55031 | 571.3 | 19.0 |
| 8800.72591 | 639.8 | 31.6 |
| 8801.59100 | 700.8 | 23.0 |
| 8802.56096 | 727.4 | 16.3 |
| 8802.63289 | 742.6 | 20.2 |
| 8804.53716 | 736.6 | 15.0 |
| 8804.62272 | 700.5 | 10.8 |
| 8812.53006 | 592.9 | 26.9 |
| 8812.61004 | 287.6 | 29.5 |
| 8817.61384 | −182.2 | 19.5 |
| 8832.56591 | −703.8 | 21.0 |
| 8833.55323 | −737.5 | 24.9 |
| 8833.64288 | −546.5 | 20.6 |
| 8835.59108 | −569.5 | 20.0 |
| 8861.53040 | 688.1 | 15.7 |
| HIP 005763 | | |
| 8078.56772* | −61.9 | 11.3 |
| 8079.58427 | −53.6 | 7.5 |
| 8080.62024 | −45.4 | 9.6 |
| 8453.58523 | 38.4 | 12.8 |
| 8454.56220 | 36.6 | 11.2 |
| 8455.59389 | 47.7 | 8.6 |
| 8480.55554 | 34.9 | 11.4 |
| 8486.53386 | 34.0 | 9.2 |
| 8699.82914 | 16.6 | 9.3 |
| 8702.89324 | 14.5 | 10.1 |
| 8705.86816 | −15.1 | 9.7 |
| 8761.66765 | −16.6 | 9.3 |
| 8761.70735 | −10.6 | 14.1 |
| 8767.69761 | −39.7 | 30.0 |
| 8772.64876 | −30.3 | 15.7 |
| 8776.67979 | −35.1 | 16.6 |
| 8804.59023 | 0.5 | 11.7 |
| 8829.55582 | −2.5 | 15.6 |

**Table A2**
(Continued)

| BJD − 2,450,000 (days) | RV ($m s^{-1}$) | $\sigma_{RV}$ ($m s^{-1}$) |
|---|---|---|
| 8835.55624 | −12.1 | 11.5 |
| HIP 034222 | | |
| 8103.73297* | −9.8 | 16.1 |
| 8105.74962 | −28.0 | 10.2 |
| 8107.73982 | −38.4 | 20.9 |
| 8148.64093 | 1.8 | 11.4 |
| 8149.62949 | 36.4 | 9.5 |
| 8150.66532 | 19.3 | 14.2 |
| 8467.76467 | 19.6 | 15.2 |
| 8469.73676 | 10.2 | 11.9 |
| 8545.54512 | −30.7 | 17.0 |
| 8547.55476 | −27.9 | 17.6 |
| 8583.47349 | −38.5 | 13.9 |
| 8584.48261 | −17.5 | 11.5 |
| 8798.86694 | 65.1 | 22.3 |
| 8806.81245 | 34.2 | 21.7 |
| 8814.78550 | 60.3 | 22.1 |
| 8819.80890 | 36.6 | 26.1 |
| 8827.77791 | 53.3 | 22.6 |
| 8831.77616 | 33.8 | 18.0 |
| 8836.74275 | 7.2 | 13.4 |
| HIP 086221 | | |
| 7948.62058* | 62.1 | 18.2 |
| 8299.68175 | 108.2 | 20.5 |
| 8303.67192 | 79.7 | 39.2 |
| 8709.57041 | −58.1 | 22.5 |
| 8712.55082 | −93.9 | 15.9 |
| 8716.56836 | −123.7 | 15.8 |
| 8738.47559 | −30.1 | 13.1 |
| 8740.47209 | 50.1 | 21.8 |
| 8741.47443 | −63.6 | 15.5 |

**Note.** (*) marks the reference epoch.

**Table A3**
Sample of 198 K Dwarfs with RV Curves

| HIP | R.A. (hh:mm:ss.sss) | Decl. (°:′:″) | Parallax (mas) | $V$ (mag) | $K$ (mag) | $V - K$ (mag) | $M_V$ (mag) | $\mathrm{MAD_{RV}}$ ($\mathrm{m\,s^{-1}}$) | No. Obs. | Time Span (days) |
|---|---|---|---|---|---|---|---|---|---|---|
| K Dwarf RV Standards | | | | | | | | | | |
| 3535 | 00:45:04.894 | +01:47:07.88 | 46.37 | 8.01 | 5.74 | 2.26 | 6.34 | 15.2 | 77 | 892 |
| 58345 | 11:57:56.207 | −27:42:25.37 | 98.45 | 6.97 | 4.53 | 2.44 | 6.93 | 9.8 | 62 | 733 |
| 73184 | 14:57:28.001 | −21:24:55.71 | 171.22 | 5.75 | 3.80 | 1.94 | 6.91 | 10.3 | 77 | 56 |
| K Dwarfs with Known Planets | | | | | | | | | | |
| 2350 | 00:29:59.873 | −05:45:50.40 | 20.03 | 9.37 | 7.31 | 2.06 | 5.88 | 39.5 | 24 | 34 |
| 57370 | 11:45:42.292 | +02:49:17.33 | 33.74 | 8.05 | 6.15 | 1.90 | 5.70 | 42.0 | 20 | 30 |
| 72339 | 14:47:32.727 | −00:16:53.31 | 31.54 | 8.04 | 6.23 | 1.81 | 5.53 | 75.6 | 27 | 42 |
| 98505 | 20:00:43.713 | +22:42:39.06 | 51.41 | 7.66 | 5.54 | 2.12 | 6.22 | 129.0 | 31 | 40 |
| 99711 | 20:13:59.846 | −00:52:00.77 | 51.77 | 7.76 | 5.54 | 2.22 | 6.33 | 40.4 | 32 | 40 |
| K Dwarfs with New Planet Candidates | | | | | | | | | | |
| 65 | 00:00:44.905 | −54:49:49.85 | 18.28 | 11.13 | 8.29 | 2.84 | 7.44 | 430.3 | 58 | 491 |
| 5763 | 01:13:58.867 | +16:29:40.27 | 34.16 | 9.86 | 6.91 | 2.95 | 7.53 | 28.7 | 19 | 756 |
| 34222 | 07:05:42.243 | +27:28:14.99 | 41.89 | 10.23 | 6.78 | 3.45 | 8.34 | 29.0 | 19 | 733 |
| 86221 | 17:37:10.761 | +27:53:47.12 | 33.91 | 9.20 | 6.30 | 2.90 | 6.85 | 72.2 | 9 | 792 |
| K Dwarfs with Flat RV Curves | | | | | | | | | | |
| 112 | 00:01:25.840 | −16:56:54.40 | 31.13 | 10.53 | 7.22 | 3.31 | 7.99 | 12.5 | 8 | 377 |
| 897 | 00:11:04.612 | −05:47:02.30 | 39.15 | 10.77 | 7.12 | 3.65 | 8.74 | 18.6 | 17 | 855 |
| 974 | 00:12:04.024 | +27:05:56.23 | 37.93 | 8.69 | 6.30 | 2.39 | 6.58 | 12.0 | 8 | 379 |
| 1539 | 00:19:12.397 | −03:03:13.01 | 32.31 | 10.99 | 7.46 | 3.53 | 8.54 | 24.4 | 12 | 758 |
| 3493 | 00:44:37.150 | −18:56:48.20 | 31.81 | 10.69 | 7.12 | 3.56 | 8.20 | 26.3 | 10 | 404 |
| 3998 | 00:51:21.754 | +18:44:21.31 | 46.79 | 9.21 | 6.24 | 2.97 | 7.56 | 11.3 | 13 | 408 |
| 4022 | 00:51:34.020 | −22:54:36.24 | 63.96 | 8.94 | 5.74 | 3.21 | 7.97 | 12.1 | 16 | 408 |
| 4061 | 00:52:00.062 | +20:34:58.32 | 31.37 | 11.36 | 7.63 | 3.74 | 8.85 | 23.0 | 12 | 788 |
| 4353 | 00:55:49.255 | −29:40:33.44 | 32.82 | 9.44 | 6.57 | 2.87 | 7.02 | 9.8 | 7 | 378 |
| 4691 | 01:00:18.490 | −25:36:52.74 | 31.70 | 9.92 | 7.21 | 2.71 | 7.43 | 8.0 | 9 | 368 |
| 4824 | 01:01:57.040 | −09:53:08.01 | 30.55 | 10.39 | 7.29 | 3.10 | 7.82 | 16.9 | 13 | 751 |
| 5027 | 01:04:24.152 | −25:36:17.99 | 41.66 | 9.84 | 6.84 | 3.00 | 7.94 | 7.8 | 16 | 400 |
| 5286 | 01:07:37.872 | +22:57:17.92 | 47.50 | 8.41 | 5.76 | 2.65 | 6.79 | 15.6 | 13 | 399 |
| 5957 | 01:16:39.357 | +25:19:53.30 | 42.31 | 10.11 | 6.66 | 3.46 | 8.24 | 14.9 | 9 | 394 |
| 6037 | 01:17:34.025 | −15:30:11.96 | 33.19 | 9.75 | 7.17 | 2.58 | 7.36 | 6.5 | 7 | 407 |
| 6342 | 01:21:29.379 | +24:19:50.04 | 38.54 | 10.62 | 7.11 | 3.51 | 8.55 | 7.0 | 8 | 394 |
| 6390 | 01:22:07.613 | −26:53:35.17 | 33.83 | 8.74 | 6.50 | 2.24 | 6.39 | 12.2 | 9 | 486 |
| 6558 | 01:24:16.527 | +12:54:27.12 | 30.67 | 9.46 | 7.06 | 2.40 | 6.89 | 9.7 | 7 | 379 |
| 6639 | 01:25:09.490 | −01:03:34.84 | 30.76 | 9.44 | 6.92 | 2.52 | 6.88 | 16.8 | 12 | 724 |
| 7228 | 01:33:09.124 | −24:54:51.62 | 30.00 | 10.00 | 7.17 | 2.84 | 7.39 | 14.5 | 9 | 380 |
| 7500 | 01:36:39.523 | +21:33:47.21 | 30.92 | 9.29 | 6.88 | 2.41 | 6.74 | 25.9 | 11 | 729 |
| 8043 | 01:43:15.973 | +27:50:31.56 | 47.23 | 10.30 | 6.60 | 3.70 | 8.67 | 16.1 | 13 | 845 |
| 8543 | 01:50:07.880 | +29:27:52.47 | 39.04 | 8.05 | 6.11 | 1.95 | 6.01 | 14.9 | 8 | 392 |
| 9716 | 02:04:59.327 | −15:40:41.17 | 39.06 | 7.77 | 5.88 | 1.88 | 5.72 | 14.4 | 9 | 380 |
| 10312 | 02:12:51.011 | −17:41:12.21 | 37.24 | 10.74 | 7.34 | 3.40 | 8.59 | 26.8 | 9 | 344 |
| 11083 | 02:22:41.647 | +18:24:38.35 | 30.55 | 8.79 | 6.63 | 2.16 | 6.21 | 8.1 | 8 | 298 |
| 11707 | 02:31:03.278 | +08:22:55.16 | 30.37 | 10.91 | 7.55 | 3.35 | 8.32 | 22.2 | 8 | 781 |
| 11759 | 02:31:42.472 | −15:16:24.45 | 35.86 | 8.66 | 6.40 | 2.26 | 6.43 | 13.7 | 8 | 391 |
| 12493 | 02:40:42.873 | +01:11:55.24 | 42.91 | 9.53 | 6.50 | 3.03 | 7.69 | 14.0 | 6 | 387 |
| 13065 | 02:47:55.873 | +28:42:44.20 | 36.46 | 10.84 | 7.48 | 3.36 | 8.65 | 27.6 | 8 | 746 |
| 13079 | 02:48:06.530 | −11:45:47.39 | 33.76 | 10.85 | 7.22 | 3.62 | 8.49 | 15.0 | 8 | 367 |
| 14445 | 03:06:26.737 | +01:57:54.63 | 68.94 | 9.04 | 5.65 | 3.39 | 8.23 | 9.4 | 11 | 377 |
| 16242 | 03:29:19.795 | −11:40:42.12 | 45.28 | 9.98 | 6.45 | 3.54 | 8.26 | 9.0 | 7 | 300 |
| 17496 | 03:44:51.125 | +11:55:12.01 | 44.32 | 9.12 | 6.20 | 2.91 | 7.35 | 12.4 | 8 | 350 |
| 19441 | 04:09:49.349 | +09:18:19.79 | 32.27 | 10.17 | 7.26 | 2.91 | 7.72 | 14.0 | 7 | 366 |
| 20232 | 04:20:10.586 | −14:45:39.85 | 34.58 | 9.88 | 6.83 | 3.05 | 7.58 | 8.1 | 7 | 380 |
| 20240 | 04:20:14.241 | −09:02:13.46 | 31.88 | 9.69 | 7.13 | 2.56 | 7.20 | 18.7 | 9 | 781 |
| 21489 | 04:36:54.310 | −14:53:12.16 | 30.44 | 9.95 | 7.20 | 2.75 | 7.36 | 13.3 | 15 | 423 |
| 22715 | 04:53:04.731 | +22:14:06.62 | 37.68 | 8.78 | 6.29 | 2.49 | 6.66 | 9.4 | 7 | 379 |
| 23431 | 05:02:09.831 | +14:04:53.63 | 33.33 | 8.18 | 6.32 | 1.86 | 5.80 | 18.8 | 8 | 768 |
| 24454 | 05:14:48.133 | +00:39:43.08 | 37.47 | 10.02 | 6.99 | 3.02 | 7.88 | 10.3 | 6 | 395 |
| 24783 | 05:18:47.191 | −21:23:37.55 | 50.28 | 9.33 | 6.15 | 3.18 | 7.84 | 13.9 | 11 | 434 |
| 24819 | 05:19:12.658 | −03:04:25.72 | 64.73 | 7.84 | 5.05 | 2.79 | 6.89 | 11.1 | 16 | 517 |

**Table A3**
(Continued)

| HIP | R.A. (hh:mm:ss.sss) | Decl. (°:′:″) | Parallax (mas) | $V$ (mag) | $K$ (mag) | $V-K$ (mag) | $M_V$ (mag) | $MAD_{RV}$ ($ms^{-1}$) | No. Obs. | Time Span (days) |
|---|---|---|---|---|---|---|---|---|---|---|
| 24874 | 05:19:59.577 | −15:50:22.72 | 41.15 | 8.70 | 6.21 | 2.50 | 6.78 | 14.2 | 10 | 375 |
| 26175 | 05:34:48.620 | −23:28:08.34 | 37.56 | 8.79 | 6.48 | 2.31 | 6.67 | 11.5 | 9 | 423 |
| 26844 | 05:41:58.867 | +15:20:14.01 | 46.83 | 10.57 | 6.88 | 3.69 | 8.92 | 19.3 | 9 | 376 |
| 26907 | 05:42:45.836 | +02:40:44.55 | 30.31 | 8.57 | 6.43 | 2.14 | 5.98 | 5.9 | 6 | 396 |
| 27397 | 05:48:17.139 | −11:08:04.64 | 37.39 | 10.94 | 7.28 | 3.66 | 8.81 | 10.5 | 12 | 368 |
| 28494 | 06:00:53.972 | +21:01:15.58 | 32.79 | 9.97 | 7.00 | 2.97 | 7.54 | 10.5 | 5 | 394 |
| 28921 | 06:06:16.615 | −27:54:20.99 | 31.15 | 8.98 | 6.78 | 2.20 | 6.45 | 9.1 | 8 | 367 |
| 29132 | 06:08:40.712 | +09:28:41.69 | 30.41 | 10.36 | 7.33 | 3.03 | 7.78 | 12.2 | 13 | 380 |
| 29208 | 06:09:35.911 | +05:40:08.03 | 34.73 | 8.37 | 6.27 | 2.10 | 6.08 | 13.5 | 10 | 380 |
| 29875 | 06:17:25.837 | +17:59:21.13 | 30.18 | 10.41 | 7.17 | 3.24 | 7.80 | 12.8 | 9 | 337 |
| 30893 | 06:29:05.528 | +27:00:31.96 | 33.66 | 8.61 | 6.36 | 2.25 | 6.24 | 9.3 | 9 | 368 |
| 31069 | 06:31:11.083 | +05:52:36.96 | 32.17 | 8.94 | 6.74 | 2.20 | 6.47 | 10.8 | 10 | 367 |
| 32530 | 06:47:15.778 | −18:15:31.39 | 31.17 | 10.57 | 7.20 | 3.37 | 8.04 | 9.6 | 9 | 355 |
| 34317 | 07:06:52.109 | +23:58:08.25 | 31.32 | 10.07 | 7.13 | 2.94 | 7.55 | 10.2 | 8 | 362 |
| 34414 | 07:08:04.238 | +29:50:04.18 | 44.93 | 8.33 | 6.06 | 2.28 | 6.60 | 9.0 | 9 | 423 |
| 34423 | 07:08:09.306 | −09:58:07.32 | 35.17 | 8.84 | 6.51 | 2.33 | 6.57 | 10.9 | 10 | 407 |
| 34673 | 07:10:49.579 | −14:25:58.93 | 40.58 | 9.90 | 6.63 | 3.27 | 7.94 | 15.0 | 8 | 436 |
| 34950 | 07:13:53.112 | +25:00:40.97 | 40.56 | 8.38 | 6.22 | 2.16 | 6.42 | 19.6 | 7 | 785 |
| 35851 | 07:23:29.253 | −20:01:24.23 | 32.12 | 9.84 | 6.94 | 2.90 | 7.37 | 9.7 | 9 | 410 |
| 35872 | 07:23:47.066 | +12:57:52.99 | 41.72 | 8.18 | 5.89 | 2.30 | 6.28 | 17.6 | 9 | 449 |
| 38492 | 07:52:59.602 | +22:33:22.99 | 31.60 | 11.07 | 7.60 | 3.47 | 8.57 | 23.1 | 24 | 396 |
| 38702 | 07:55:23.921 | −15:29:53.20 | 31.20 | 10.68 | 7.66 | 3.02 | 8.15 | 16.7 | 7 | 404 |
| 38992 | 07:58:50.384 | +10:07:47.13 | 33.05 | 8.09 | 6.18 | 1.91 | 5.69 | 8.5 | 9 | 396 |
| 39068 | 07:59:35.632 | +12:58:59.04 | 30.43 | 8.33 | 6.46 | 1.87 | 5.75 | 6.9 | 8 | 404 |
| 39826 | 08:08:13.186 | +21:06:18.26 | 60.09 | 9.45 | 6.08 | 3.36 | 8.34 | 13.2 | 11 | 408 |
| 42074 | 08:34:31.651 | −00:43:33.83 | 47.31 | 7.31 | 5.42 | 1.88 | 5.68 | 13.2 | 33 | 517 |
| 43233 | 08:48:26.156 | +06:28:06.08 | 39.55 | 10.59 | 6.99 | 3.60 | 8.58 | 20.8 | 12 | 410 |
| 43771 | 08:54:57.243 | −24:23:39.44 | 32.11 | 8.65 | 6.46 | 2.19 | 6.18 | 13.9 | 10 | 406 |
| 44072 | 08:58:38.181 | +20:32:48.29 | 47.85 | 9.24 | … | … | 7.64 | 14.3 | 8 | 396 |
| 44109 | 08:59:02.245 | +01:51:52.89 | 32.28 | 10.44 | 7.19 | 3.25 | 7.99 | 29.9 | 11 | 396 |
| 44526 | 09:04:20.694 | −15:54:51.30 | 35.34 | 8.76 | 6.39 | 2.37 | 6.50 | 16.7 | 13 | 424 |
| 44920 | 09:09:03.265 | +27:25:55.35 | 32.71 | 10.29 | 7.20 | 3.09 | 7.87 | 7.8 | 8 | 396 |
| 46549 | 09:29:35.053 | −05:22:21.74 | 41.24 | 9.79 | 6.52 | 3.27 | 7.87 | 10.4 | 7 | 369 |
| 47201 | 09:37:11.340 | +22:41:38.92 | 45.57 | 9.40 | 6.34 | 3.06 | 7.69 | 12.0 | 9 | 411 |
| 47261 | 09:37:58.332 | +22:31:23.18 | 31.05 | 9.72 | 6.85 | 2.86 | 7.18 | 16.8 | 16 | 424 |
| 48016 | 09:47:16.685 | +01:34:36.95 | 32.70 | 10.98 | 7.56 | 3.42 | 8.55 | 17.4 | 12 | 412 |
| 48024 | 09:47:22.400 | +26:18:12.56 | 30.95 | 10.92 | 7.34 | 3.58 | 8.38 | 17.8 | 10 | 395 |
| 48447 | 09:52:39.162 | +03:07:48.58 | 43.96 | 10.52 | 7.08 | 3.45 | 8.74 | 9.8 | 10 | 414 |
| 49127 | 10:01:37.295 | −15:25:29.24 | 37.13 | 8.65 | 6.21 | 2.44 | 6.50 | 20.0 | 11 | 466 |
| 49429 | 10:05:26.519 | +26:29:16.10 | 34.13 | 9.10 | 6.65 | 2.45 | 6.77 | 11.6 | 8 | 429 |
| 49544 | 10:06:56.863 | +02:57:51.88 | 44.33 | 9.92 | 6.39 | 3.53 | 8.16 | 11.1 | 9 | 432 |
| 50657 | 10:20:43.406 | −01:28:11.38 | 31.11 | 9.39 | 6.76 | 2.63 | 6.85 | 9.5 | 11 | 412 |
| 50782 | 10:22:09.488 | +11:18:36.86 | 37.97 | 7.77 | 5.91 | 1.86 | 5.67 | 11.9 | 11 | 424 |
| 51254 | 10:28:10.444 | +06:44:06.45 | 39.67 | 8.49 | 6.26 | 2.23 | 6.48 | 8.1 | 9 | 412 |
| 51931 | 10:36:30.792 | −13:50:35.82 | 31.01 | 8.72 | 6.57 | 2.15 | 6.18 | 14.9 | 10 | 375 |
| 52708 | 10:46:36.902 | −24:35:07.74 | 46.49 | 9.33 | 6.44 | 2.89 | 7.67 | 9.3 | 9 | 378 |
| 52765 | 10:47:19.207 | +21:29:51.06 | 30.43 | 10.00 | 7.16 | 2.84 | 7.42 | 12.0 | 7 | 335 |
| 53486 | 10:56:30.798 | +07:23:18.51 | 57.79 | 7.35 | 5.20 | 2.15 | 6.16 | 14.4 | 9 | 412 |
| 54651 | 11:11:10.701 | −10:57:03.19 | 49.38 | 9.24 | 6.33 | 2.91 | 7.71 | 4.5 | 9 | 401 |
| 54810 | 11:13:13.235 | +04:28:56.43 | 54.70 | 8.68 | 5.85 | 2.82 | 7.37 | 8.2 | 10 | 408 |
| 54922 | 11:14:48.171 | −23:06:17.72 | 43.39 | 9.00 | 6.03 | 2.97 | 7.18 | 8.3 | 8 | 446 |
| 55066 | 11:16:22.146 | −14:41:36.13 | 55.82 | 10.01 | 6.46 | 3.56 | 8.75 | 14.0 | 7 | 469 |
| 55119 | 11:17:07.508 | −27:48:48.71 | 56.52 | 9.72 | 6.20 | 3.52 | 8.48 | 5.5 | 7 | 406 |
| 55772 | 11:25:39.948 | +20:00:07.68 | 32.19 | 8.31 | 6.35 | 1.96 | 5.85 | 7.7 | 9 | 348 |
| 55988 | 11:28:27.748 | +07:31:02.19 | 36.50 | 10.20 | 7.06 | 3.14 | 8.02 | 10.6 | 9 | 383 |
| 56570 | 11:35:49.367 | +24:36:42.53 | 30.21 | 9.35 | 6.87 | 2.48 | 6.75 | 15.8 | 6 | 432 |
| 56578 | 11:35:59.172 | +16:58:05.72 | 31.40 | 9.48 | 6.84 | 2.64 | 6.97 | 7.6 | 5 | 52 |
| 56838 | 11:39:08.164 | −27:41:46.37 | 32.73 | 9.91 | 6.91 | 3.00 | 7.49 | 12.7 | 5 | 66 |
| 57866 | 11:52:08.338 | +18:45:18.66 | 37.95 | 8.39 | 6.27 | 2.12 | 6.28 | 6.1 | 7 | 444 |
| 58293 | 11:57:16.291 | −26:08:29.02 | 37.13 | 8.91 | 6.41 | 2.50 | 6.76 | 10.2 | 5 | 66 |
| 58374 | 11:58:11.705 | −23:55:25.99 | 39.02 | 8.68 | 6.31 | 2.36 | 6.63 | 8.0 | 7 | 382 |
| 58863 | 12:04:17.458 | +09:11:35.00 | 30.84 | 9.83 | 7.06 | 2.77 | 7.28 | 7.9 | 3 | 2 |
| 58949 | 12:05:12.529 | −01:30:32.53 | 30.97 | 8.17 | 6.32 | 1.85 | 5.62 | 8.1 | 3 | 4 |

**Table A3**
(Continued)

| HIP | R.A. (hh:mm:ss.sss) | Decl. (°:′:″) | Parallax (mas) | $V$ (mag) | $K$ (mag) | $V-K$ (mag) | $M_V$ (mag) | $\mathrm{MAD_{RV}}$ ($\mathrm{ms^{-1}}$) | No. Obs. | Time Span (days) |
|---|---|---|---|---|---|---|---|---|---|---|
| 60207 | 12:20:46.831 | −19:53:45.83 | 34.43 | 8.96 | 6.59 | 2.37 | 6.65 | 14.9 | 8 | 345 |
| 60343 | 12:22:21.273 | +25:10:11.89 | 33.43 | 11.07 | 7.60 | 3.47 | 8.69 | 4.5 | 3 | 4 |
| 61329 | 12:33:59.744 | −14:38:19.19 | 38.21 | 9.11 | 6.44 | 2.67 | 7.02 | 6.6 | 7 | 299 |
| 63467 | 13:00:16.996 | −02:42:17.22 | 37.89 | 9.74 | 6.77 | 2.97 | 7.63 | 16.4 | 14 | 307 |
| 65574 | 13:26:39.557 | −24:17:36.14 | 33.08 | 8.81 | 6.56 | 2.25 | 6.41 | 10.1 | 6 | 56 |
| 66675 | 13:40:07.131 | −04:11:09.96 | 67.58 | 9.59 | 6.04 | 3.56 | 8.74 | 11.0 | 9 | 347 |
| 67092 | 13:45:05.340 | −04:37:13.23 | 39.84 | 10.50 | 7.20 | 3.30 | 8.50 | 19.7 | 8 | 355 |
| 67105 | 13:45:14.717 | +08:50:09.52 | 47.65 | 8.46 | 5.97 | 2.49 | 6.85 | 13.2 | 8 | 395 |
| 67211 | 13:46:19.025 | −00:27:29.04 | 30.75 | 9.30 | 6.91 | 2.39 | 6.74 | 6.2 | 5 | 51 |
| 67291 | 13:47:28.801 | +06:18:56.36 | 32.49 | 10.03 | 7.01 | 3.01 | 7.59 | 12.9 | 8 | 408 |
| 67344 | 13:48:10.056 | −10:47:19.50 | 32.05 | 8.35 | 6.43 | 1.92 | 5.87 | 15.0 | 6 | 54 |
| 69410 | 14:12:41.562 | +23:48:51.49 | 30.03 | 8.88 | 6.44 | 2.43 | 6.26 | 9.0 | 10 | 373 |
| 69485 | 14:13:31.194 | −06:57:32.33 | 51.64 | 10.08 | 6.57 | 3.51 | 8.64 | 15.3 | 8 | 369 |
| 70218 | 14:21:57.216 | +29:37:46.63 | 69.70 | 8.53 | 5.42 | 3.10 | 7.74 | 11.8 | 9 | 424 |
| 70472 | 14:24:49.861 | −17:27:08.09 | 31.38 | 10.79 | 7.28 | 3.51 | 8.27 | 18.3 | 8 | 417 |
| 70529 | 14:25:43.475 | +23:37:01.51 | 61.11 | 9.62 | 5.97 | 3.65 | 8.56 | 8.8 | 16 | 277 |
| 70956 | 14:30:47.718 | −08:38:46.81 | 58.87 | 9.38 | 5.77 | 3.61 | 8.22 | 7.8 | 8 | 392 |
| 71190 | 14:33:34.902 | +09:20:03.76 | 30.88 | 8.78 | 6.59 | 2.19 | 6.23 | 9.5 | 6 | 54 |
| 71914 | 14:42:33.648 | +19:28:47.22 | 46.34 | 9.07 | 5.82 | 3.24 | 7.40 | 12.1 | 16 | 270 |
| 72044 | 14:44:11.991 | +22:11:07.16 | 38.54 | 9.82 | 6.90 | 2.92 | 7.75 | 12.8 | 10 | 410 |
| 72200 | 14:46:03.072 | +27:30:44.45 | 39.73 | 7.95 | 5.98 | 1.97 | 5.94 | 11.3 | 7 | 353 |
| 72237 | 14:46:23.282 | +16:29:48.14 | 58.00 | 9.20 | 6.06 | 3.13 | 8.01 | 8.1 | 16 | 313 |
| 73066 | 14:55:55.019 | −27:07:38.25 | 36.36 | 8.94 | 6.48 | 2.46 | 6.74 | 12.2 | 18 | 318 |
| 73457 | 15:00:43.411 | −11:08:06.47 | 51.70 | 9.42 | 5.99 | 3.43 | 7.98 | 9.9 | 8 | 325 |
| 73512 | 15:01:29.974 | +15:52:07.99 | 32.99 | 9.13 | 6.58 | 2.55 | 6.72 | 8.0 | 5 | 40 |
| 73786 | 15:04:53.525 | +05:38:17.19 | 53.80 | 9.83 | 6.47 | 3.37 | 8.49 | 9.8 | 18 | 314 |
| 74555 | 15:13:59.641 | −03:47:52.79 | 37.04 | 9.87 | 6.91 | 2.97 | 7.72 | 19.6 | 7 | 381 |
| 74981 | 15:19:21.154 | +29:12:22.25 | 38.02 | 10.30 | 7.10 | 3.20 | 8.20 | 21.4 | 4 | 417 |
| 75201 | 15:22:04.101 | −04:46:38.82 | 52.92 | 9.39 | 6.18 | 3.21 | 8.01 | 18.8 | 8 | 324 |
| 75672 | 15:27:38.020 | +10:35:39.08 | 39.01 | 9.83 | 6.65 | 3.18 | 7.79 | 6.4 | 5 | 316 |
| 75686 | 15:27:42.697 | +02:35:51.93 | 37.96 | 10.26 | 6.90 | 3.36 | 8.16 | 16.0 | 6 | 326 |
| 76779 | 15:40:34.570 | −18:02:56.50 | 64.28 | 8.91 | 5.69 | 3.23 | 7.95 | 12.0 | 9 | 283 |
| 77908 | 15:54:38.429 | −26:00:15.03 | 41.00 | 9.20 | 6.24 | 2.96 | 7.26 | 8.6 | 13 | 333 |
| 78336 | 15:59:42.293 | −05:04:34.50 | 30.27 | 9.08 | 6.83 | 2.24 | 6.48 | 13.4 | 8 | 413 |
| 79066 | 16:08:24.487 | −13:08:07.81 | 35.43 | 8.67 | 6.38 | 2.29 | 6.41 | 10.5 | 5 | 333 |
| 80366 | 16:24:19.810 | −13:38:29.97 | 46.46 | 8.33 | 6.00 | 2.33 | 6.67 | 14.1 | 14 | 327 |
| 80539 | 16:26:33.482 | +15:39:53.83 | 37.09 | 10.55 | 7.20 | 3.35 | 8.40 | 23.1 | 6 | 329 |
| 80597 | 16:27:20.393 | +00:55:29.68 | 32.82 | 9.95 | 6.79 | 3.16 | 7.53 | 10.5 | 6 | 313 |
| 81030 | 16:32:57.882 | −12:35:30.23 | 30.53 | 10.60 | 7.25 | 3.35 | 8.03 | 10.0 | 7 | 417 |
| 84487 | 17:16:20.234 | −12:10:41.36 | 36.73 | 10.20 | 6.91 | 3.29 | 8.03 | 15.3 | 10 | 798 |
| 85561 | 17:29:06.558 | −23:50:10.02 | 53.02 | 9.63 | 6.39 | 3.24 | 8.26 | 6.3 | 16 | 328 |
| 87464 | 17:52:16.606 | −07:33:37.46 | 33.35 | 10.01 | 6.97 | 3.03 | 7.62 | 8.3 | 6 | 36 |
| 87745 | 17:55:24.781 | +03:45:16.22 | 38.13 | 10.18 | 6.82 | 3.36 | 8.09 | 16.0 | 9 | 799 |
| 87768 | 17:55:44.899 | +18:30:01.41 | 39.93 | 9.22 | 6.30 | 2.92 | 7.23 | 11.8 | 7 | 822 |
| 88961 | 18:09:32.246 | −00:19:37.66 | 33.40 | 8.97 | 6.54 | 2.42 | 6.58 | 12.3 | 14 | 802 |
| 88962 | 18:09:33.263 | −12:02:20.01 | 36.29 | 10.43 | 6.99 | 3.44 | 8.23 | 20.1 | 10 | 799 |
| 89517 | 18:16:02.252 | +13:54:48.19 | 55.01 | 10.09 | 6.56 | 3.53 | 8.79 | 12.3 | 18 | 328 |
| 89656 | 18:17:49.804 | +26:40:16.70 | 31.74 | 9.59 | 6.95 | 2.64 | 7.10 | 23.6 | 5 | 31 |
| 89728 | 18:18:40.679 | −06:42:03.73 | 32.42 | 9.26 | 6.72 | 2.54 | 6.82 | 6.4 | 7 | 339 |
| 89825 | 18:19:50.842 | −01:56:18.98 | 51.12 | 9.60 | 6.28 | 3.32 | 8.15 | 8.8 | 19 | 329 |
| 90611 | 18:29:22.303 | −27:58:19.02 | 33.90 | 9.37 | 6.49 | 2.88 | 7.02 | 7.6 | 5 | 29 |
| 90626 | 18:29:31.914 | +09:03:43.52 | 36.20 | 8.61 | 6.33 | 2.28 | 6.40 | 11.1 | 10 | 789 |
| 90959 | 18:33:17.760 | +22:18:51.30 | 43.53 | 8.89 | 6.16 | 2.73 | 7.08 | 9.4 | 19 | 329 |
| 92311 | 18:48:51.872 | +17:26:20.22 | 58.82 | 9.17 | 5.92 | 3.25 | 8.01 | 14.0 | 16 | 355 |
| 93195 | 18:58:56.491 | −00:30:14.34 | 32.41 | 8.36 | 6.38 | 1.97 | 5.91 | 10.6 | 8 | 758 |
| 93731 | 19:05:07.515 | +23:04:40.06 | 31.46 | 8.53 | 6.62 | 1.91 | 6.02 | 5.7 | 6 | 66 |
| 94650 | 19:15:35.054 | +11:33:16.98 | 38.07 | 8.04 | 5.94 | 2.10 | 5.95 | 16.3 | 7 | 727 |
| 95299 | 19:23:16.463 | −06:35:07.32 | 34.72 | 9.71 | 6.81 | 2.90 | 7.42 | 9.4 | 7 | 745 |
| 95429 | 19:24:42.094 | +08:32:59.76 | 30.30 | 11.34 | 7.73 | 3.61 | 8.75 | 27.6 | 8 | 501 |
| 95730 | 19:28:15.396 | +12:32:09.24 | 35.69 | 9.19 | 6.35 | 2.84 | 6.95 | 11.0 | 6 | 405 |
| 95890 | 19:30:05.478 | +21:40:34.01 | 32.67 | 9.90 | 7.07 | 2.83 | 7.47 | 8.2 | 4 | 44 |
| 96121 | 19:32:37.919 | +00:34:39.05 | 44.52 | 10.43 | 6.81 | 3.62 | 8.67 | 14.0 | 18 | 412 |
| 96285 | 19:34:39.841 | +04:34:57.05 | 69.32 | 9.35 | 5.92 | 3.43 | 8.55 | 10.5 | 17 | 412 |

**Table A3**
(Continued)

| HIP | R.A. (hh:mm:ss.sss) | Decl. (°:′:″) | Parallax (mas) | $V$ (mag) | $K$ (mag) | $V-K$ (mag) | $M_V$ (mag) | $\mathrm{MAD_{RV}}$ ($\mathrm{ms^{-1}}$) | No. Obs. | Time Span (days) |
|---|---|---|---|---|---|---|---|---|---|---|
| 97805 | 19:52:29.915 | −23:56:57.06 | 36.77 | 9.41 | 6.61 | 2.81 | 7.24 | 16.8 | 6 | 488 |
| 98828 | 20:04:10.046 | +25:47:24.82 | 45.56 | 7.81 | 5.64 | 2.17 | 6.10 | 13.3 | 15 | 430 |
| 99205 | 20:08:24.367 | +06:40:43.46 | 39.23 | 9.84 | 6.93 | 2.91 | 7.80 | 22.3 | 8 | 208 |
| 99332 | 20:09:41.013 | −03:07:44.43 | 30.94 | 9.55 | 6.74 | 2.81 | 7.01 | 14.3 | 9 | 165 |
| 102115 | 20:41:40.697 | −05:29:34.25 | 31.53 | 10.66 | 7.23 | 3.42 | 8.15 | 27.0 | 8 | 439 |
| 102226 | 20:42:49.360 | +20:50:40.61 | 39.93 | 8.24 | 6.01 | 2.23 | 6.25 | 11.2 | 5 | 460 |
| 102332 | 20:44:00.655 | −21:21:20.87 | 40.05 | 9.89 | 6.75 | 3.14 | 7.90 | 10.5 | 14 | 345 |
| 102582 | 20:47:16.841 | +10:51:36.47 | 31.94 | 9.78 | 7.00 | 2.78 | 7.31 | 11.6 | 9 | 540 |
| 104329 | 21:08:01.902 | +25:10:34.44 | 30.59 | 9.83 | 7.06 | 2.77 | 7.26 | 12.4 | 7 | 507 |
| 109807 | 22:14:26.748 | +02:42:24.12 | 34.12 | 10.31 | 7.49 | 2.82 | 7.98 | 18.7 | 10 | 736 |
| 112918 | 22:52:02.520 | +23:24:47.67 | 38.17 | 9.76 | 6.82 | 2.94 | 7.67 | 16.6 | 13 | 811 |
| 113333 | 22:57:07.357 | +28:00:07.03 | 36.03 | 9.83 | 7.02 | 2.81 | 7.62 | 10.1 | 5 | 339 |
| 114941 | 23:16:51.829 | +05:41:45.59 | 39.59 | 10.51 | 6.80 | 3.71 | 8.49 | 18.3 | 12 | 896 |
| 115752 | 23:27:04.836 | −01:17:10.58 | 32.98 | 10.48 | 7.01 | 3.46 | 8.07 | 12.4 | 12 | 514 |
| 117463 | 23:49:01.159 | +03:10:52.20 | 38.94 | 8.41 | 6.17 | 2.24 | 6.36 | 9.4 | 13 | 464 |
| 117779 | 23:53:08.595 | +29:01:05.05 | 44.41 | 9.71 | 6.39 | 3.32 | 7.95 | 13.9 | 19 | 412 |
| 118086 | 23:57:14.381 | −16:30:27.37 | 32.61 | 11.01 | 7.60 | 3.41 | 8.57 | 17.7 | 10 | 878 |

## ORCID iDs

Leonardo A. Paredes https://orcid.org/0000-0003-1324-0495
Todd J. Henry https://orcid.org/0000-0002-9061-2865
Samuel N. Quinn https://orcid.org/0000-0002-8964-8377
Douglas R. Gies https://orcid.org/0000-0001-8537-3583
Hodari-Sadiki James https://orcid.org/0000-0003-4568-2079
Wei-Chun Jao https://orcid.org/0000-0003-0193-2187
Russel J. White https://orcid.org/0000-0001-5313-7498

## References

Baglin, A., Auvergne, M., Barge, P., et al. 2006, in The CoRoT Mission Pre-Launch Status—Stellar Seismology and Planet Finding, ESA Special Publication, Vol. 1306, ed. M. Fridlund et al. (Noordwijk: ESA Publications), 33
Bakos, G. Á., Pál, A., Latham, D. W., Noyes, R. W., & Stefanik, R. P. 2006, ApJL, 641, L57
Baranec, C., Riddle, R., Ramaprakash, A. N., et al. 2012, Proc. SPIE, 8447, 844704
Baranne, A., Queloz, D., Mayor, M., et al. 1996, A&AS, 119, 373
Bernstein, R., Shectman, S. A., Gunnels, S. M., Mochnacki, S., & Athey, A. E. 2003, Proc. SPIE, 4841, 1694
Borucki, W. J., Koch, D., Basri, G., et al. 2010, Sci, 327, 977
Bouchy, F., Udry, S., Mayor, M., et al. 2005, A&A, 444, L15
Brewer, J. M., Giguere, M., & Fischer, D. A. 2014, PASP, 126, 48
Butler, R. P., Vogt, S. S., Laughlin, G., et al. 2017, AJ, 153, 208
Crane, J. D., Shectman, S. A., & Butler, R. P. 2006, Proc. SPIE, 6269, 626931
Cuntz, M., & Guinan, E. F. 2016, ApJ, 827, 79
Evans, D. W., Riello, M., De Angeli, F., et al. 2018, A&A, 616, A4
Ge, J., van Eyken, J., Mahadevan, S., et al. 2006, ApJ, 648, 683
Giguere, M. J., Fischer, D. A., Payne, M. J., et al. 2015, ApJ, 799, 89
Giguere, M. J., Fischer, D. A., Zhang, C. X. Y., et al. 2016, ApJ, 824, 150
Gilbert, J., Bergmann, C., Bloxham, G., et al. 2018, Proc. SPIE, 10702, 107020Y
Gould, A., & Chanamé, J. 2004, ApJS, 150, 455
Gray, R. O., & Corbally, Christopher J. 2009, Stellar Spectral Classification (Princeton, NJ: Princeton Univ. Press)
Guilluy, G., Andretta, V., Borsa, F., et al. 2020, A&A, 639, A49
Guilluy, G., Sozzetti, A., Brogi, M., et al. 2019, A&A, 625, A107
Halbwachs, J. L., Mayor, M., & Udry, S. 2005, A&A, 431, 1129
Henry, G. W., Donahue, R. A., & Baliunas, S. L. 2002, ApJL, 577, L111
Henry, T. J., Ianna, P. A., Kirkpatrick, J. D., & Jahreiss, H. 1997, AJ, 114, 388
Henry, T. J., Jao, W.-C., Subasavage, J. P., et al. 2006, AJ, 132, 2360
Henry, T. J., Jao, W.-C., Winters, J. G., et al. 2018, AJ, 155, 265
Henry, T. J., & McCarthy, Donald W., J. 1993, AJ, 106, 773
Hinkel, N. R., Kane, S. R., Henry, G. W., et al. 2015, ApJ, 803, 8
Høg, E., Fabricius, C., Makarov, V. V., et al. 2000, A&A, 355, L27
Horch, E. P., Veillette, D. R., Baena Gallé, R., et al. 2009, AJ, 137, 5057
Howell, S. B., Sobeck, C., Haas, M., et al. 2014, PASP, 126, 398
Kaufer, A., & Pasquini, L. 1998, Proc. SPIE, 3355, 844
Latham, D. W., Mazeh, T., Stefanik, R. P., Mayor, M., & Burki, G. 1989, Natur, 339, 38
Malkov, O. Y., Tamazian, V. S., Docobo, J. A., & Chulkov, D. A. 2012, A&A, 546, A69
Mamajek, E. E. 2012, arXiv:1210.1616
Mason, B. D., Douglass, G. G., & Hartkopf, W. I. 1999, AJ, 117, 1023
Mason, B. D., Wycoff, G. L., Hartkopf, W. I., Douglass, G. G., & Worley, C. E. 2001, AJ, 122, 3466
Mayor, M., Marmier, M., Lovis, C., et al. 2011, arXiv:1109.2497
Mayor, M., Pepe, F., Queloz, D., et al. 2003, Msngr, 114, 20
Mayor, M., & Queloz, D. 1995, Natur, 378, 355
Meschiari, S., Wolf, A. S., Rivera, E., et al. 2009, PASP, 121, 1016
Moutou, C., Mayor, M., Bouchy, F., et al. 2005, A&A, 439, 367
Munari, U., & Walter, F. M. 2016, MNRAS, 455, L57
Nielsen, L. D., Brahm, R., Bouchy, F., et al. 2020, A&A, 639, A76
Nusdeo, Daniel A. 2018, in AAS Meeting, 231, 244.13
Oh, S., Price-Whelan, A. M., Hogg, D. W., Morton, T. D., & Spergel, D. N. 2017, AJ, 153, 257
Oliva, E., Origlia, L., Baffa, C., et al. 2006, Proc. SPIE, 6269, 626919
Piskunov, N. E., & Valenti, J. A. 2002, A&A, 385, 1095
Pourbaix, D., Tokovinin, A. A., Batten, A. H., et al. 2004, A&A, 424, 727
Raghavan, D., McAlister, H. A., Henry, T. J., et al. 2010, ApJS, 190, 1
Redfield, S., Endl, M., Cochran, W. D., & Koesterke, L. 2008, ApJL, 673, L87
Ricker, G. R., Winn, J. N., Vanderspek, R., et al. 2014, Proc. SPIE, 9143, 914320
Riddle, R. L., Tokovinin, A., Mason, B. D., et al. 2015, ApJ, 799, 4
Roberts, Lewis C., J., Tokovinin, A., Mason, B. D., et al. 2015, AJ, 149, 118
Santos, N. C., Mayor, M., Naef, D., et al. 2000, A&A, 356, 599
Santos, N. C., Udry, S., Mayor, M., et al. 2003, A&A, 406, 373
Skrutskie, M. F., Cutri, R. M., Stiening, R., et al. 2006, AJ, 131, 1163
Shaya, E. J., & Olling, R. P. 2011, ApJS, 192, 2
Söderhjelm, S. 1999, A&A, 341, 121
Subasavage, J. P., Bailyn, C. D., Smith, R. C., et al. 2010, Proc. SPIE, 7737, 77371C
Tala, M., Berdja, A., Jones, M., et al. 2014, Proc. SPIE, 9147, 914789
Tokovinin, A. 2014, AJ, 147, 87
Tokovinin, A., Fischer, D. A., Bonati, M., et al. 2013, PASP, 125, 1336
Udry, S., Mayor, M., Naef, D., et al. 2000, A&A, 356, 590
van Leeuwen, F. 2007, A&A, 474, 653
Vogt, S. S., Allen, S. L., Bigelow, B. C., et al. 1994, Proc. SPIE, 2198, 362
Wittenmyer, R. A., Endl, M., Cochran, W. D., Levison, H. F., & Henry, G. W. 2009, ApJS, 182, 97
Wittrock, J. M., Kane, S. R., Horch, E. P., et al. 2016, AJ, 152, 149
Wolszczan, A., & Frail, D. A. 1992, Natur, 355, 145
Wright, J. T., & Eastman, J. D. 2014, PASP, 126, 838
Zucker, S. 2003, MNRAS, 342, 1291